



**HAL**  
open science

## **Extensive H<sub>2</sub>O degassing in deeply erupted submarine glasses inferred from Samoan melt inclusions: The EM2 mantle source is damp, not dry**

Olivia E Anderson, Matthew G Jackson, Ayla S Pamukçu, Estelle F. Rose-Koga, Véronique Le Roux, Frieder Klein, Kenneth T. Koga, Glenn A Gaetani, Allison A Price

### ► To cite this version:

Olivia E Anderson, Matthew G Jackson, Ayla S Pamukçu, Estelle F. Rose-Koga, Véronique Le Roux, et al.. Extensive H<sub>2</sub>O degassing in deeply erupted submarine glasses inferred from Samoan melt inclusions: The EM2 mantle source is damp, not dry. *Chemical Geology*, 2024, 651, pp.121979. 10.1016/j.chemgeo.2024.121979 . insu-04516946

**HAL Id: insu-04516946**

**<https://insu.hal.science/insu-04516946v1>**

Submitted on 22 Mar 2024

**HAL** is a multi-disciplinary open access archive for the deposit and dissemination of scientific research documents, whether they are published or not. The documents may come from teaching and research institutions in France or abroad, or from public or private research centers.

L'archive ouverte pluridisciplinaire **HAL**, est destinée au dépôt et à la diffusion de documents scientifiques de niveau recherche, publiés ou non, émanant des établissements d'enseignement et de recherche français ou étrangers, des laboratoires publics ou privés.

1 **Extensive H<sub>2</sub>O degassing in deeply erupted submarine glasses inferred from**  
2 **Samoan melt inclusions: The EM2 mantle source is damp, not dry**

3 **O. E. Anderson<sup>1\*</sup>, M. G. Jackson<sup>1</sup>, A. S. Pamukçu<sup>2,3</sup>, E. F. Rose-Koga<sup>4</sup>, V. Le Roux<sup>2</sup>, F.**  
4 **Klein<sup>2</sup>, K. T. Koga<sup>4</sup>, G. A. Gaetani<sup>2</sup>, A. A. Price<sup>1</sup>**

5 <sup>1</sup>Isotope Geochemistry Facility – Global Center for Mantle Zoology (GCMZ), University of  
6 California Santa Barbara, Department of Earth Science, Santa Barbara, CA, USA <sup>2</sup>Woods Hole  
7 Oceanographic Institution, Woods Hole, Massachusetts 02543, USA <sup>3</sup>Geological Sciences,  
8 Stanford University, Stanford, CA, USA <sup>4</sup>Institut des Sciences de la Terre d'Orléans (ISTO),  
9 UO/CNRS/BRGM, 1A rue de la Férellerie, 45071, Orléans, France

10 \*Corresponding author: Olivia E. Anderson ([anderson03@ucsb.edu](mailto:anderson03@ucsb.edu))  
11

12 **Highlights:**

- 13
- 14 ● Samoan melt inclusions have higher H<sub>2</sub>O/Ce—indicating less degassing—compared to  
15 Samoan pillow glasses.
  - 16
  - 17 ● High <sup>87</sup>Sr/<sup>86</sup>Sr melt inclusions have high H<sub>2</sub>O/Ce, contrary to prior observations using  
18 pillow glasses.
  - 19
  - 20 ● Low H<sub>2</sub>O/Ce in high <sup>87</sup>Sr/<sup>86</sup>Sr glasses indicates extensive degassing has occurred, so  
21 cannot be used to infer mantle H<sub>2</sub>O/Ce.
  - 22
  - 23 ● Melt inclusions show that enriched mantle (EM) lavas have H<sub>2</sub>O/Ce similar to non-EM  
24 lavas.
  - 25
  - 26 ● Elevated CO<sub>2</sub> in EM melts leads to greater degassing and lower H<sub>2</sub>O/Ce in erupted  
27 glasses compared to depleted mantle.
  - 28
  - 29
- 30
- 31
- 32
- 33

34 Find the final version of the article at:

35  
36 Anderson, O.E., Jackson, M.G., Pamukçu, A.S., Rose-Koga, E.F., Le Roux, V., Klein, F., Koga,  
37 K.T., Gaetani, G.A. and Price, A.A. (2024). Extensive H<sub>2</sub>O degassing in deeply erupted  
38 submarine glasses inferred from Samoan melt inclusions: The EM2 mantle source is damp, not  
39 dry. *Chemical Geology*, 651, 121979. <https://doi.org/10.1016/j.chemgeo.2024.121979>

40 **Abstract**

41 Submarine glasses erupted at intraplate volcanic hotspot settings sampling enriched mantle  
42 (EM)—characterized by high  $^{87}\text{Sr}/^{86}\text{Sr}$ —exhibit lower  $\text{H}_2\text{O}/\text{Ce}$  than glasses representing less  
43 enriched mantle domains, leading to the interpretation that the EM mantle is  $\text{H}_2\text{O}$ -poor (“dry”).  
44 We test whether low  $\text{H}_2\text{O}/\text{Ce}$  observed in pillow glasses of EM lavas resulted from degassing of  
45 higher  $\text{H}_2\text{O}/\text{Ce}$  primary melts by measuring  $\text{H}_2\text{O}/\text{Ce}$  and  $^{87}\text{Sr}/^{86}\text{Sr}$  in olivine-hosted melt  
46 inclusions from two deeply-erupted (3950 and 2190 meters below sea level (mbsl)) Samoan  
47 submarine lavas from Vailulu‘u and Malumalu seamounts. Vailulu‘u ( $\text{H}_2\text{O}/\text{Ce}=161\text{--}275$ ) and  
48 Malumalu (149–232) melt inclusions have an average  $\text{H}_2\text{O}/\text{Ce}$  ( $197\pm 58$  2SD,  $N=15$ ) that is  
49 nearly twice as high as  $\text{H}_2\text{O}/\text{Ce}$  in pillow glasses from these two seamounts (average  
50  $\text{H}_2\text{O}/\text{Ce}=106\pm 51$ ,  $N=65$ ). Notably, the average  $\text{H}_2\text{O}/\text{Ce}$  of Samoan melt inclusions ( $197\pm 58$ ) is  
51 comparable to pillow glasses from non-EM hotspots. We show that lower  $\text{H}_2\text{O}/\text{Ce}$  in submarine  
52 Samoan glasses compared to melt inclusions results from greater closed-system degassing, and  
53 concomitant loss of  $\text{H}_2\text{O}$ , because EM melts have higher initial concentrations of  $\text{CO}_2$ . We show  
54 that the lower  $\text{H}_2\text{O}/\text{Ce}$  in global EM pillow glasses compared to non-EM pillow glasses can be  
55 modeled to be the result of more extensive degassing of  $\text{H}_2\text{O}$  in EM melts, which owes to higher  
56  $\text{CO}_2$  in primary melts (20,000–90,000 ppm) of EM sources compared to non-EM melts (300–  
57 50,000 ppm  $\text{CO}_2$ ). Instead of originating from a dry mantle, we conclude that EM lavas derive  
58 from a damp mantle, but EM melts lose more  $\text{H}_2\text{O}$  by degassing than non-EM melts.

59 **Keywords:** melt inclusion, Samoa, hotspot, degassing, enriched mantle,  $\text{H}_2\text{O}$

60

61

**62 1. Introduction**

63 Although volatiles are a minor component in silicate melts, they play an outsize role on  
64 the properties and behavior of magmatic systems. Hydrogen and carbon affect the rheology of  
65 the mantle, the depth and extent of melting, the composition of melts, and how melts evolve  
66 (e.g., Asimow & Langmuir, 2003; Gaetani & Grove, 1998; Hirschmann, 2006; Hirth &  
67 Kohlstedt, 1996, 2003; Portnyagin et al., 2007). Therefore, connecting volatile element  
68 compositions to mantle domains characterized by particular isotopic compositions, such as  
69 enriched mantle (EM), can provide additional insights into mantle heterogeneities. A variety of  
70 geochemical “flavors” have been identified in the mantle via geochemical taxonomy of ocean  
71 island basalts (OIB), and the various mantle species are broadly encompassed by several  
72 canonical mantle endmembers that include HIMU (high  $\mu=^{238}\text{U}/^{204}\text{Pb}$ ), EM1 (enriched mantle 1),  
73 EM2 (enriched mantle 2), and DM (depleted mantle). Samoan lavas have unique geochemical  
74 signatures that extend to Enriched Mantle 2 (EM2) isotopic compositions (e.g., high  $^{87}\text{Sr}/^{86}\text{Sr}$ ,  
75 intermediate  $^{206}\text{Pb}/^{204}\text{Pb}$ , and low  $^{143}\text{Nd}/^{144}\text{Nd}$ ). The EM2 mantle source has been suggested to be  
76 derived from recycled continental materials (e.g., White & Hofmann, 1982; White & Duncan,  
77 1996; Jackson & Macdonald, 2022). Therefore, characterization of Samoan EM2 lavas can  
78 provide insights into the role that deep continental crust subduction plays in controlling the  
79 volatile budgets of the mantle.

80 The ratios  $\text{H}_2\text{O}/\text{La}$  or  $\text{H}_2\text{O}/\text{Ce}$  measured in submarine glasses are commonly used to  
81 evaluate  $\text{H}_2\text{O}$  enrichment or depletion in the mantle because  $\text{H}_2\text{O}$ , La, and Ce have similar  
82 degrees of incompatibility (e.g., Michael, 1995). Thus, their ratios are not significantly affected  
83 by partial melting and crystal fractionation. The EM2 mantle source has been interpreted to be  
84 ‘dry’ because the  $\text{H}_2\text{O}/\text{Ce}$  (or  $\text{H}_2\text{O}/\text{La}$ ) is lower at higher  $^{87}\text{Sr}/^{86}\text{Sr}$  for Samoan glasses (Workman

85 et al., 2006). Workman et al. (2006) found that  $H_2O/La$  anticorrelates with  $^{87}Sr/^{86}Sr$ : the more  
86 geochemically enriched (higher  $^{87}Sr/^{86}Sr$ ) Samoan glasses have lower  $H_2O/La$  than more  
87 geochemically depleted Samoan glasses; the high  $H_2O/La$  MORB mantle endmember anchors  
88 the low  $^{87}Sr/^{86}Sr$  portion of the array. Workman et al. (2006) explained this relationship between  
89  $^{87}Sr/^{86}Sr$  and  $H_2O/La$  as the result of diffusive  $H_2O$  loss from EM2 reservoirs during long-term  
90 storage in a dry and depleted mantle, resulting in a “dry” EM2 mantle domain that has low  
91  $H_2O/La$  and low  $H_2O$ . Similarly, Dixon et al. (2002) found that high  $^{87}Sr/^{86}Sr$  basalts erupted in  
92 MOR settings had low  $H_2O/Ce$ . However, unlike Workman et al. (2006), Dixon et al. (2002)  
93 suggested that the dry nature of the EM reservoir was due to dehydration of sediments during  
94 subduction, resulting in low  $H_2O/Ce$  signatures in subducted, dehydrated sediments, which  
95 ultimately contribute to enriched mantle domains. Bizimis and Peslier (2015) offered further  
96 discussion regarding the origin of apparently dry EM2 domains and argued that the low  $H_2O/Ce$   
97 in EM lavas is the result of recycling of pyroxenite-bearing oceanic lithosphere. The pyroxenites  
98 they examined have low  $H_2O/Ce$  and high  $H_2O$ , a result of preferential partitioning of Ce into  
99 clinopyroxene compared to  $H_2O$ .

100 Additional work highlights the low  $H_2O/Ce$  in enriched mantle domains (Kendrick et al.,  
101 2017). In particular, classical EM1 and EM2 oceanic hotspots—Pitcairn and Societies,  
102 respectively—exhibit negative correlations between  $^{87}Sr/^{86}Sr$  and  $H_2O/Ce$  in submarine glasses  
103 (Kendrick et al., 2014). Thus, low  $H_2O/Ce$  appears to be a defining feature of EM lavas, and  
104 constraining the origin of this geochemical signature is critical for understanding the origin of the  
105 EM mantle and/or the petrogenesis of EM lavas.

106 Existing models for the origin of low  $H_2O/La$  and  $H_2O/Ce$  in EM-flavored OIB pillow  
107 glasses quenched in deep submarine environments are predicated on the assumption that the low

108 H<sub>2</sub>O/Ce is a source feature and the EM primary melts have low H<sub>2</sub>O/Ce inherited from the  
109 mantle source (Dixon et al., 2002; Dixon & Clague, 2001; Wallace, 2002; Workman et al., 2006;  
110 Kendrick et al., 2014). This interpretation assumes that magmatic degassing follows open system  
111 behavior, a mechanism that results in significant loss of CO<sub>2</sub>, but not H<sub>2</sub>O, from the melt by  
112 degassing: the H<sub>2</sub>O/Ce in deeply erupted glasses (i.e.,  $\geq 0.1$  kbar; Workman et al., 2006) resulting  
113 from this process are similar to the mantle source despite having degassed most of their  
114 magmatic CO<sub>2</sub>.

115 In this study, we test this assumption using combined H<sub>2</sub>O/Ce and <sup>87</sup>Sr/<sup>86</sup>Sr  
116 measurements in individual olivine-hosted melt inclusions isolated from two well-characterized  
117 submarine Samoan basalts that were characterized by Workman et al. (2006). We present  
118 volatile (H<sub>2</sub>O, CO<sub>2</sub>, Cl, F, S), major, and trace element concentrations and <sup>87</sup>Sr/<sup>86</sup>Sr on Samoan  
119 melt inclusions from both samples—AVON3-78-1 and AVON3-71-2—which were obtained  
120 from Malumalu and Vailulu‘u seamounts, respectively. Malumalu lavas reach <sup>87</sup>Sr/<sup>86</sup>Sr of up to  
121 0.708901, which is the most extreme EM2 composition that we explore in this study. In contrast,  
122 Vailulu‘u lavas have <sup>87</sup>Sr/<sup>86</sup>Sr that range from 0.705352 to 0.706720, and thus represent a less  
123 enriched composition at the Samoan hotspot. Previous <sup>87</sup>Sr/<sup>86</sup>Sr analyses of Samoan melt  
124 inclusions demonstrated extreme heterogeneity (0.70434 to 0.70926) that has been verified using  
125 both *in situ* LA-ICP-MS approach (laser-ablation inductively coupled plasma mass spectrometry;  
126 Jackson & Hart, 2006) and an approach involving wet chemistry followed by TIMS (thermal  
127 ionization mass spectrometry; Reinhard et al., 2018). Critically for this study, the melt inclusions  
128 from the two lavas examined here span nearly the same range of <sup>87</sup>Sr/<sup>86</sup>Sr (0.704858–0.709225)  
129 as identified in prior melt inclusion studies (Jackson & Hart, 2006; Reinhard et al., 2018) and  
130 have similar trace element characteristics as the Samoan glasses examined for H<sub>2</sub>O/La and

131  $^{87}\text{Sr}/^{86}\text{Sr}$  by Workman et al. (2006) (0.704521–0.708901). We interpret this to indicate that the  
132 melt inclusions thus sample the same mantle sources as the pillow glasses studied by Workman  
133 et al. (2006).

134         However, Samoan melt inclusions in this study exhibit two key differences with the  
135 Samoan submarine glasses reported in Workman et al. (2006): 1) the melt inclusions have higher  
136  $\text{H}_2\text{O}/\text{Ce}$  than Samoan submarine glasses and 2) the inclusions exhibit no relationship between  
137  $\text{H}_2\text{O}/\text{Ce}$  and  $^{87}\text{Sr}/^{86}\text{Sr}$ , which contrasts with the negative correlation between  $^{87}\text{Sr}/^{86}\text{Sr}$  and  
138  $\text{H}_2\text{O}/\text{Ce}$  observed in Samoan pillow glasses. We model the difference in  $\text{H}_2\text{O}/\text{Ce}$  between melt  
139 inclusions and pillow glasses as being a result of closed-system degassing, a mechanism that  
140 results in greatly diminished  $\text{CO}_2$  and  $\text{H}_2\text{O}$  concentrations in the melt (in contrast to open-system  
141 degassing, which results in greatly diminished  $\text{CO}_2$ , but not  $\text{H}_2\text{O}$ , melt concentrations). In this  
142 model, the melt inclusions experience less closed-system degassing compared to submarine  
143 glasses because of deep entrapment of the melt inclusions in growing olivine crystals within  
144 magma chambers. Melts that were not trapped continued to degas both  $\text{CO}_2$  and  $\text{H}_2\text{O}$  up until  
145 eruption and quenching on the seafloor, resulting in lower  $\text{H}_2\text{O}/\text{Ce}$  in the submarine glasses  
146 compared to the deeply entrapped melt inclusions.

147         We also present a model suggesting that, across global oceanic hotspots, primary melts  
148 with higher  $^{87}\text{Sr}/^{86}\text{Sr}$  (e.g., Samoan and Societies EM2 glasses, Pitcairn EM1 glasses) have  
149 higher primary melt  $\text{CO}_2$  than lower  $^{87}\text{Sr}/^{86}\text{Sr}$  melts (e.g., Foundation, Hawai‘i (Lō‘ihi), and  
150 Easter hotspots). Higher  $\text{CO}_2$  in high  $^{87}\text{Sr}/^{86}\text{Sr}$  (EM) melts results in greater degassing of both  
151  $\text{CO}_2$  and  $\text{H}_2\text{O}$  (and a greater reduction in the  $\text{H}_2\text{O}/\text{Ce}$  ratio) compared to low  $^{87}\text{Sr}/^{86}\text{Sr}$  melts,  
152 which explains the negative global correlation between  $\text{H}_2\text{O}/\text{Ce}$  and  $^{87}\text{Sr}/^{86}\text{Sr}$  in OIB glasses.  
153 This new result suggests that submarine glasses sourcing EM domains do not provide reliable

154 records for evaluating the H<sub>2</sub>O and H<sub>2</sub>O/Ce in the mantle source. In melt inclusions, degassing is  
155 arrested at great depth, making it possible to identify H<sub>2</sub>O/Ce ratios that are closer to values in  
156 the primary melt.

## 157       **2. Methods**

158       Submarine pillow basalt samples in this study are from two Samoan seamounts (Figure 1)  
159 that are young (<8 ka; Sims et al., 2008) and associated with visually fresh lavas: Malumalu  
160 (sample AVON3-78-1; 2260–2190 mbsl) and Vailulu‘u (sample AVON3-71-2; 4420–3950  
161 mbsl) are olivine-rich lavas with glassy chill margins on the pillow rims. Olivine-hosted melt  
162 inclusions from Vailulu‘u and Malumalu seamounts in this study were rehomogenized on a  
163 heating stage (see supplement for methods), and these rehomogenized inclusions were then  
164 characterized for <sup>87</sup>Sr/<sup>86</sup>Sr (15 melt inclusions total), <sup>143</sup>Nd/<sup>144</sup>Nd (only three melt inclusions),  
165 stable hydrogen isotope ratios (δD), and major, trace and volatile element concentrations (Table  
166 S1). This supplement also includes methodological details for the glass major element (electron  
167 microprobe), volatile (ion probe), hydrogen isotope (ion probe), and trace element (LA-ICP-MS)  
168 analyses and the host olivine major element (electron microprobe) analyses. Strontium separation  
169 chemistry and <sup>87</sup>Sr/<sup>86</sup>Sr analyses by TIMS used in this study follow the same procedure as  
170 described in Anderson et al. (2021). The supplement includes details of Nd separation chemistry  
171 for melt inclusions, and <sup>143</sup>Nd/<sup>144</sup>Nd analyses by TIMS at the University of California, Santa  
172 Barbara Isotope Geochemistry Facility. Only three melt inclusions (all from the Vailulu‘u  
173 Seamount sample) in this study had sufficient Nd for the isotopic analysis.

174       The results of *in situ* analyses (of δD, and major, trace and volatile element concentrations)  
175 of geologic reference materials (ALV519-4-1, ALV1833-1, GL07 D52-5, and BCR-2) can be



176 found in Table S2, and  $^{87}\text{Sr}/^{86}\text{Sr}$  and  $^{143}\text{Nd}/^{144}\text{Nd}$  analyses of BCR-2 can be found in Tables S6  
177 and S8.

178 Melt inclusion major, trace, and volatile element concentrations were corrected for post-  
179 entrapment crystallization (PEC) by addition or subtraction of equilibrium olivine in 0.1%  
180 increments until the major element composition of the inclusion is in equilibrium with the host  
181 olivine forsterite (Fo) content. In the calculation, two assumptions are made: (i) the olivine-melt  
182 Fe-Mg  $K_d = 0.30$  (Roeder & Emslie, 1970; Ford et al., 1983;  $K_d = (\text{Fe}^{2+}/\text{Mg})_{\text{olivine}}/(\text{Fe}^{2+}/\text{Mg})_{\text{melt}}$ )  
183 and (ii)  $\text{Fe}^{3+}$  comprises 10% of the total moles of iron in the melt (following Hauri, 1996).  
184 Unless stated otherwise, all major, trace, and volatile element concentrations reported below  
185 have been corrected for equilibrium olivine addition/subtraction so that the inclusion is in  
186 equilibrium with the host olivine.

187 The supplement also details the method of accounting for all  $\text{CO}_2$  within a melt inclusion,  
188 including both the  $\text{CO}_2$  in the glass analyzed by ion probe, the  $\text{CO}_2$  contained within the vapor  
189 bubble obtained by Raman spectroscopy, and the volumes of bubble and glass for each melt  
190 inclusion obtained by X-ray computed microtomography (see Table S3 for the method of  
191 reconstructing the total  $\text{CO}_2$  content of each melt inclusion).

192

### 193 **3. Methods for data treatment**

194 We use a series of criteria to identify inclusions where the volatile contents have been  
195 compromised. This way the results and discussion can focus on primary magmatic signatures.  
196 Figure 2 shows all melt inclusions from which we collected volatile data. Inclusions whose  
197 volatile contents were likely compromised are designated with a black “x” in Figure 2. We do

198 not consider these inclusions further in our data analysis and interpretation so as to focus on  
199 primary magmatic signatures. However, one inclusion with exceptionally high Cl concentration  
200 (1.90 wt.% Cl) is included in subsequent analysis, but it is identified in all plots where it is  
201 shown.

202 Inclusions are excluded if they show evidence of being affected by one or more of the following:

203 i) *Diffusive proton loss.* Hydrogen isotopes can indicate whether H<sub>2</sub>O loss from the melt  
204 inclusion has occurred by proton diffusion through the host olivine. Melt inclusions  
205 that have been affected by proton diffusion will have low H<sub>2</sub>O contents and high  $\delta D$   
206 values due to faster diffusion of hydrogen over deuterium (Hauri, 2002; Gaetani et al.,  
207 2012; Bucholz et al., 2013; Hartley et al., 2015). Therefore, we measured  $\delta D$  on all  
208 melt inclusions reported in this study. Melt inclusions in the Malumalu sample  
209 (AVON3-78-1) have a  $\delta D$  range of -51.8‰ to +127.6‰, and melt inclusions in the  
210 Vailulu‘u sample (AVON3-71-2) have a  $\delta D$  range of -52.4‰ to -22.0‰ (Figure 2).  
211 Diffusive H<sub>2</sub>O loss from melt inclusions should produce a systematic relationship  
212 between melt inclusion  $\delta D$  and volume. Melt inclusions from both lavas with  
213 volumes  $>10^5 \mu\text{m}^3$  exhibit no systematic relationship between  $\delta D$  and melt inclusion  
214 volume, and they exhibit a relatively narrow range in  $\delta D$  of  $-35.8 \pm 17.0\%$  (2SD,  
215  $N=19$ ). However, the two melt inclusions with positive  $\delta D$  values, both from  
216 Malumalu (samples AVON3-78-1#13 and AVON3-78-1#32), have the smallest  
217 volumes ( $\sim 8.8 \times 10^4 \mu\text{m}^3$  and  $4.3 \times 10^4 \mu\text{m}^3$ ). Prior work has shown that smaller  
218 volume melt inclusions are more susceptible to diffusive proton loss that results in  
219 elevated  $\delta D$  (Hauri, 2002; Gaetani et al., 2012; Bucholz et al., 2013; Hartley et al.,  
220 2015). Therefore, the two small-volume inclusions are excluded.

- 221 ii) *Breaching*. Two melt inclusions have likely suffered breaching because CO<sub>2</sub> is <200  
222 ppm and H<sub>2</sub>O is <1 wt. % (see Figure S4; AVON3-78-1#25, AVON3-78-1#37). Both  
223 melt inclusions exhibit melt-filled cracks that intersect the melt inclusions, which is  
224 strong physical evidence that supports the breaching interpretation.
- 225 iii) *Extremely large vapor bubbles*. Three melt inclusions (AVON3-78-1#10, AVON3-  
226 78-1#28, AVON3-71-2#20) have vapor bubbles that make up >10 vol. % of the melt  
227 inclusion and are excluded. Prior work suggested that large vapor bubbles result from  
228 simultaneous entrapment of a mix of melt and CO<sub>2</sub> fluid (e.g. Anderson, 1974;  
229 Frezzotti, 2001; Hanyu et al., 2020; Moore et al., 2015), which is not representative of  
230 melt-only compositions.
- 231 iv) *No CO<sub>2</sub> detected by Raman*. No Fermi doublets were observed by Raman  
232 spectroscopy for two melt inclusions (AVON3-71-2#14, AVON3-71-2#18), thus the  
233 CO<sub>2</sub> densities may have been too low for detection. To err on the side of caution, we  
234 are excluding these two melt inclusions from the interpretations of this study. For  
235 other excluded melt inclusions, CO<sub>2</sub> densities in the vapor bubbles were highly  
236 uncertain (AVON3-71-2#20; ±0.092) or so low that negative values resulted from the  
237 calibration (AVON3-78-1#25, AVON3-78-1#37, AVON3-71-2#14), and the volatile  
238 data for these four melt inclusions are excluded from the discussion (except for  
239 AVON3-71-2#14, which has an unusually high Cl concentration and is identified in  
240 each plot where it is shown).
- 241 v) *Carbonate detected by Raman*. If carbon exists as carbonate in a melt inclusion, the  
242 CO<sub>2</sub> budget of the melt inclusion may be underestimated. In this study, carbonates

243 were detected by Raman in two Malumalu melt inclusions (AVON3-78-1#15 and  
244 AVON3-78-1#32), and volatile data for these inclusions are excluded.

245

## 246 4. Results

### 247 4.1 Hydrogen and strontium isotopes

248 After filtering the data for the compromised melt inclusions, the Samoan melt inclusions  
249 from Malumalu ( $-37.8 \pm 13.2\%$ ,  $N=9$ ) and Vailulu'u ( $-33.9 \pm 19.7\%$ ,  $N=10$ ) are relatively  
250 homogenous in  $\delta D$  with an average  $\delta D$  value of  $-35.8\%$  ( $\pm 17.0\%$ , 2SD,  $N=19$ ). The Samoan  
251 inclusions have heavier  $\delta D$  than most MORB and Lō'ihī (now known as Kama'ehuakanaloa)  
252 values, consistent with heavy  $\delta D$  values (ca.  $-40\%$ ) found in OIBs with recycled components  
253 (Loewen et al., 2019).

254 Critically,  $^{87}\text{Sr}/^{86}\text{Sr}$  measurements in melt inclusions provide a test for whether the Samoan  
255 melt inclusions of this study represent the Samoan mantle sources sampled by Vailulu'u and  
256 Malumalu glasses. If they do represent the same sources, then the volatile and trace element  
257 concentrations of the melt inclusions can be directly compared to concentration measurements in  
258 Samoan pillow lava glasses. The  $^{87}\text{Sr}/^{86}\text{Sr}$  range for all of the Malumalu (sample AVON3-78-1)  
259 melt inclusions reported here is large, from 0.706594 to 0.709225 (Figure 3, 4). The inclusions  
260 largely fall within the range reported for Malumalu pillow glasses and whole rocks (0.706374–  
261 0.708901; Workman et al., 2006). The  $^{87}\text{Sr}/^{86}\text{Sr}$  range for all of the Vailulu'u (sample AVON3-  
262 71-2) melt inclusions reported here is smaller compared to AVON3-78-1 melt inclusions, from  
263 0.704858 to 0.705718. The range of Vailulu'u melt inclusion  $^{87}\text{Sr}/^{86}\text{Sr}$  overlaps with the range  
264 reported for Vailulu'u pillow glasses (0.705352–0.706720; Workman et al., 2006) but, relative to

265 Vailulu‘u pillow glasses and whole rocks, the Vailulu‘u melt inclusions are shifted to less  
266 radiogenic (lower)  $^{87}\text{Sr}/^{86}\text{Sr}$  values. Taken together, the  $^{87}\text{Sr}/^{86}\text{Sr}$  for the Malumalu and Vailulu‘u  
267 melt inclusions in this study bracket the  $^{87}\text{Sr}/^{86}\text{Sr}$  obtained pillow glasses from each volcano: the  
268 lowest  $^{87}\text{Sr}/^{86}\text{Sr}$  in the melt inclusions (0.704858) is somewhat lower than the lowest value  
269 measured in whole rocks and pillow glasses (0.705352) from these two seamounts, and the  
270 highest  $^{87}\text{Sr}/^{86}\text{Sr}$  in the melt inclusions (0.709225) is slightly higher than the highest value  
271 measured in pillow glasses (0.708901). This statement is also true for the  $(\text{La}/\text{Sm})_{\text{N}}$  and  
272  $\text{K}_2\text{O}/\text{TiO}_2$  for the melt inclusions compared to the whole rocks and pillow glasses (Figure 4).  
273 Therefore, the Malumalu and Vailulu‘u melt inclusions from these two hand samples represent  
274 the full compositional range previously identified in these volcanoes and, in fact, span nearly the  
275 entire range encountered in  $^{87}\text{Sr}/^{86}\text{Sr}$  (i.e., 0.7045 to 0.7089) for the eastern Samoan volcanic  
276 province—including Ta‘u, Vailulu‘u, and Malumalu volcanoes—examined by Workman et al.  
277 (2006). Thus, the melt inclusions can be used to interpret mantle source geochemical  
278 characteristics, including volatile budgets, of the volcanoes examined in Workman et al. (2006).

#### 279 *4.2 Volatiles*

280 After omitting melt inclusions that have been contaminated, breached, affected by hydrogen  
281 diffusion, and have unreliable  $\text{CO}_2$  analyses by Raman, the magmatic volatile content of the  
282 Samoan melt inclusions can be explored. Figure 5 provides ratios ( $\text{H}_2\text{O}/\text{Ce}$ ,  $\text{CO}_2/\text{Nb}$ ,  $\text{Cl}/\text{Nb}$ ,  
283  $\text{S}/\text{Gd}$ , and  $\text{F}/\text{Nd}$ ) of volatile ( $\text{H}_2\text{O}$ ,  $\text{CO}_2$ ,  $\text{Cl}$ ,  $\text{S}$ , and  $\text{F}$ ) to nonvolatile ( $\text{Ce}$ ,  $\text{Nb}$ ,  $\text{Gd}$ , and  $\text{Nd}$ )  
284 incompatible trace elements (ITEs) that have similar mineral-melt partition coefficients during  
285 mantle melting and magmatic differentiation processes. Below we examine the volatile  
286 concentrations and their ratios to nonvolatile ITEs.

287

288 4.2.1. CO<sub>2</sub> in Samoan melt inclusions.

289 We use the CO<sub>2</sub> concentration in the melt inclusion glass analyzed by SIMS and the CO<sub>2</sub>  
290 density in the vapor bubble from Raman spectroscopy to reconstruct the total CO<sub>2</sub> concentration  
291 of the melt inclusion. When comparing melt inclusion and vapor bubble CO<sub>2</sub>, 3 to 94 mass  
292 percent (average ~59 mass percent) of the total CO<sub>2</sub> (i.e., melt inclusion CO<sub>2</sub>+vapor bubble CO<sub>2</sub>)  
293 resides in the vapor bubble, consistent with prior findings of large CO<sub>2</sub> fractions residing in melt  
294 inclusion vapor bubbles (e.g., DeVitre et al., 2021; Aster et al., 2016; Moore et al., 2015).  
295 Malumalu and Vailulu‘u melt inclusions have relatively similar total CO<sub>2</sub> contents of 1506–5746  
296 ppm and 658–4771 ppm, respectively. The associated host pillow glasses for the Malumalu and  
297 Vailulu‘u samples have total CO<sub>2</sub> contents of 70 ppm and 179 ppm, respectively (Workman et  
298 al., 2006), which is far lower than the melt inclusions from these two volcanoes. These  
299 observations are consistent with greater CO<sub>2</sub>-H<sub>2</sub>O saturation pressures for the melt inclusions  
300 than the pillow glasses.

301 During melting and crystallization, the incompatibility (i.e., the bulk partition coefficient) of  
302 CO<sub>2</sub> is similar to Nb and Ba, thus the ratios of CO<sub>2</sub>/Nb or CO<sub>2</sub>/Ba have been used to estimate  
303 upper mantle carbon content (Hirschmann, 2018; Michael & Graham, 2015; Saal et al., 2002;  
304 Cartigny et al., 2008; Le Voyer et al., 2017). However, only undegassed, CO<sub>2</sub>-undersaturated  
305 melts will have CO<sub>2</sub>/Nb or CO<sub>2</sub>/Ba that are representative of the mantle source, but such melts  
306 are rare (Hauri et al., 2018; Graham & Michael, 2021; Le Voyer et al., 2017; Michael & Graham,  
307 2015; Saal et al., 2002). These CO<sub>2</sub>-undersaturated melts tend to be geochemically depleted  
308 (Hauri et al., 2018; Shimizu et al., 2023) and have higher CO<sub>2</sub>/Nb than most submarine volcanic  
309 glasses, which are CO<sub>2</sub>-saturated and thus degassed (e.g., the Samoan pillow glasses and melt  
310 inclusions examined here). The Samoan melt inclusions in this study have a measured CO<sub>2</sub>/Nb

311 range of 19 to 125 for Vailulu‘u melt inclusions and 27 to 133 for Malumalu melt inclusions, and  
312 such ratios are lower than inferred for mantle sources of oceanic hotspot lavas (e.g., >1000 for  
313 Iceland; Matthews et al., 2021) and MORB ( $\text{CO}_2/\text{Nb} > 283$ ; Michael & Graham, 2015). Thus,  
314 we suggest the Samoan samples are  $\text{CO}_2$ -saturated and degassed, which is consistent with highly  
315 variable total  $\text{CO}_2$  contents (658 to 5746 ppm) relative to the narrow range of Nb concentrations  
316 in our Samoan melt inclusions (Figure S6b,d). The Samoan pillow glasses from these two  
317 volcanoes have even lower (more degassed)  $\text{CO}_2$  concentrations while exhibiting similar Nb  
318 concentrations to the melt inclusions (Figure S6b,d).

319

#### 320 4.2.2. Cl in Samoan melt inclusions versus Samoa pillow glasses.

321 Malumalu melt inclusions have 651–1198 ppm Cl, and Vailulu‘u melt inclusions have 412–  
322 765 ppm Cl (excluding the high Cl inclusion AVON3-71-2#14, which has a Cl concentration of  
323 1.9 wt.% Cl). The associated pillow glasses from the two samples hosting the melt inclusions—  
324 AVON3-78-1 and AVON3-71-2—have 1004 ppm Cl and 1490 ppm Cl, respectively. The suite  
325 of pillow glasses from all Malumalu and Vailulu‘u samples have Cl contents that vary from 886  
326 to 1725 ppm and 547 to 1818 ppm, respectively.

327 To determine if any melt inclusions are influenced by the assimilation of seawater-derived  
328 materials, we use Cl/Nb as an indicator of assimilation of seawater-derived materials (e.g.,  
329 Kendrick et al., 2013, 2015; Kent et al., 1999a, 1999b, 2002). This is a useful ratio because Cl  
330 and Nb behave similarly during crystal fractionation and melting due to their similar  
331 incompatibility in basalt melts (Rowe & Lassiter, 2009). Malumalu melt inclusions have a Cl/Nb  
332 range of 14–25 and Vailulu‘u melt inclusions have a Cl/Nb range of 14–22 (excluding melt

333 inclusion sample AVON3-71-2#14, which has with  $Cl/Nb = 840$ ) (Figure 5). The Samoan melt  
334 inclusions have  $Cl/Nb$  that overlap with mid-ocean ridge basalts (MORB), where  $Cl/Nb_{MORB}$  is 5  
335 to 17 (Lassiter et al., 2002; Le Roux et al., 2006), but the Samoan inclusions tend to be shifted to  
336 higher  $Cl/Nb$ .

337 The pillow glasses for the Malumalu (AVON3-78-1) and Vailulu'u (AVON3-71-2) samples  
338 hosting the Samoan melt inclusions have  $Cl/Nb$  of 13 and 27, respectively (Kendrick et al.,  
339 2015). Both lavas have been previously suggested to have assimilated seawater-derived materials  
340 (Kendrick et al., 2014; Reinhard et al., 2018). We find some evidence for assimilation in a single  
341 melt inclusion from Vailulu'u (AVON3-71-2#14), which has a high  $Cl/Nb$  ratio of 840,  
342 suggesting contamination by seawater-derived materials; however, any such assimilation does  
343 not appear to have impacted  $^{87}Sr/^{86}Sr$  ( $0.705471 \pm 0.000022$ ) as it is at the lower end of the range  
344 observed here (Figure 5).

#### 345 4.2.3 S in Samoan melt inclusions versus Samoa pillow glasses.

346 Malumalu melt inclusions have 1786–3163 ppm S, and Vailulu'u melt inclusions have 1582–  
347 2090 ppm S. The associated host pillow glasses (AVON3-78-1 and AVON3-71-2) have 831 ppm  
348 S and 2337 ppm S, respectively. The suite of pillow glasses from all Malumalu and Vailulu'u  
349 samples have S contents varying from 781 to 2391 ppm and 1010 to 4834 ppm, respectively  
350 (Workman et al., 2006).

351 Sulfur and Gd and Dy have similar incompatibility during melting and crystal fractionation  
352 (Saal et al., 2002) when sulfide is not present, except at lower pressures when sulfur degasses.  
353 However, Samoan basalts are known to host both sulfates and sulfides (Labidi et al., 2015). The  
354 melt inclusions in this study are sulfide supersaturated (Figure S5; using the model of Fortin et



355 al., 2015 and Smythe et al., 2017)—and sulfides are in fact, observed in some of the inclusions  
356 from the two samples examined here —thus S/Gd (Figure 5) of Samoan melt inclusions in this  
357 study may have been influenced by sulfide saturation and are likely not representative of the  
358 Samoan primary melts.

359

#### 360 4.2.4. F in Samoan melt inclusions versus Samoa pillow glasses.

361 Malumalu melt inclusions have 1161–1293 ppm F, and Vailulu‘u melt inclusions have 777–  
362 1145 ppm F. The associated host pillow glasses (AVON3-78-1 and AVON3-71-2) have 1254  
363 ppm F and 903 ppm F, respectively. The suite of pillow glasses from all Malumalu and Vailulu‘u  
364 samples have F contents varying from 1173 to 1409 ppm, and 843 to 1188 ppm F, respectively  
365 (Workman et al., 2006).

366 F/Nd in melt inclusions and glasses from global datasets of MORB and OIB are suggested to  
367 be relatively constant because there is no significant F/Nd fractionation during crystallization and  
368 melting. The F/Nd values of global OIB and MORB have been estimated to be  $20.1 \pm 5.8$   
369 (Workman et al., 2006), but there is evidence for greater F/Nd variability (Koleszar et al., 2009;  
370 Shimizu et al., 2016; Jackson et al., 2015; Lassiter et al., 2002; Métrich et al., 2014; Cabral et al.,  
371 2014; Rose-Koga et al., 2012). The average F/Nd for Malumalu melt inclusions ( $30 \pm 6$  2SD,  
372  $N=9$ ) is similar to the average F/Nd for Vailulu‘u melt inclusions ( $29 \pm 14$  2SD,  $N=10$ ), but  
373 Vailulu‘u melt inclusions have more variability in F/Nd (Figure 5). Three Vailulu‘u melt  
374 inclusions (AVON3-71-2#7, #17, #22) have ~200 ppm lower F contents than the other Samoan  
375 melt inclusions, but similar Nd contents, resulting in lower F/Nd (21–23). The Samoan melt  
376 inclusion have F/Nd ( $29 \pm 11$ , 2SD,  $N=19$ ) tends to be higher than the canonical F/Nd (~21) for

377 fresh global OIB and MORB, and higher than the average pillow glass F/Nd from Malumalu  
378 ( $22 \pm 2$ , 2SD, N=17; Workman et al., 2006) and Vailulu'u ( $22 \pm 3$ , 2SD, N=48; Workman et al.,  
379 2006). However, the average F/Nd of Samoan melt inclusions overlaps within two standard  
380 deviations of the canonical F/Nd value and the F/Nd of Samoan pillow glasses. Nonetheless, the  
381 Vailulu'u melt inclusions tend to very high F/Nd up to 41. Elevated F may be characteristic of  
382 the HIMU mantle source (Hauri & Hart, 1993; Rose-Koga et al., 2017; Jackson et al., 2015), and  
383 Vailulu'u is thought to contain a small contribution from a HIMU component (Workman et al.,  
384 2004; Jackson et al., 2014). However, we do not have an explanation for the higher F/Nd in the  
385 Vailulu'u melt inclusions relative to the glasses from this seamount.

386

#### 387 4.2.5. H<sub>2</sub>O in Samoan melt inclusions versus Samoa pillow glasses.

388 Malumalu melt inclusions have 1.56–1.95 wt.% H<sub>2</sub>O, and Vailulu'u melt inclusions have 1.13–  
389 1.39 wt.% H<sub>2</sub>O. The associated host glasses from these two submarine samples tend to have  
390 lower H<sub>2</sub>O contents than the melt inclusions with 0.91 wt.% H<sub>2</sub>O (AVON3-78-1) and 1.18 wt.%  
391 H<sub>2</sub>O (AVON3-71-2), respectively. The low H<sub>2</sub>O in the AVON3-78-1 Malumalu glass sample  
392 lies within the range of H<sub>2</sub>O for pillow glass samples from Malumalu (0.89 to 1.43 wt.%), and  
393 the same applies for the AVON3-71-2 Vailulu'u glass sample as it also lies in the range of pillow  
394 glasses from this seamount (0.63 to 1.50 wt.%) (Figure 6). When the melt inclusions and pillow  
395 glasses are corrected for olivine fractionation to be in equilibrium with mantle olivine (F<sub>0.90</sub>), a  
396 figure of H<sub>2</sub>O<sub>F<sub>0.90</sub></sub> (wt.%) versus Ce<sub>F<sub>0.90</sub></sub> (ppm) shows that the melt inclusions and pillow glasses  
397 from Malumalu and Vailulu'u seamounts have similar Ce<sub>F<sub>0.90</sub></sub>, but the inclusions have H<sub>2</sub>O that is  
398 higher than the pillow glasses (Figure S6c). We also show the same plot but instead provide the

399 *measured* H<sub>2</sub>O and Ce in the glass glasses—due to uncertainties associated with the olivine  
400 correction—and find that it does not change our conclusions.

401 Consistent with this observation, the H<sub>2</sub>O/Ce range of the Malumalu AVON3-78-1 melt  
402 inclusions (149–232, average 193±47, 2SD, N=10) and the Vailulu‘u AVON3-71-2 melt  
403 inclusions (161–275, average 190±78, 2SD, N=10) are higher than the host pillow glasses, 59  
404 (for pillow glass from sample AVON3-78-1) and 123 (for pillow glass from sample AVON3-71-  
405 2), respectively. Critically, the average H<sub>2</sub>O/Ce (197±58 2SD, N=15) in the melt inclusion  
406 dataset from Malumalu and Vailulu‘u seamounts is nearly twice as high as the same ratio in the  
407 Samoan pillow glasses from these two seamounts (106±51, 2SD, N=65). This is notable because  
408 the inclusions and pillow glasses are from the same two volcanoes, span the same range of  
409 <sup>87</sup>Sr/<sup>86</sup>Sr (Figure 3), and have similar ITE ratios (Figure 4), suggesting they sample the same  
410 mantle sources. This observation that melt inclusions have higher H<sub>2</sub>O/Ce than submarine pillow  
411 glasses may relate to the fact that the Samoan melt inclusions from Malumalu and Vailulu‘u  
412 have universally higher calculated MagmaSat CO<sub>2</sub>-H<sub>2</sub>O vapor saturation pressures (Figure 3)  
413 than the submarine pillow glasses, reflective of higher entrapment pressures for the melt  
414 inclusions (>0.870 kbar) than the eruption pressures experienced by the glasses (<0.53 kbar) (see  
415 Figure 3).

416 While Workman et al. (2006) found a negative correlation between H<sub>2</sub>O/La and <sup>87</sup>Sr/<sup>86</sup>Sr for  
417 Samoan glasses, we find that the Samoan melt inclusions in this study exhibit *no correlation*  
418 between H<sub>2</sub>O/Ce and <sup>87</sup>Sr/<sup>86</sup>Sr (Figure 3, 5a, 7a), even though the melt inclusions are from two of  
419 the three volcanoes studied by Workman et al. (2006) and span the same range of <sup>87</sup>Sr/<sup>86</sup>Sr as  
420 their pillow glasses. In contrast to Workman et al. (2006), the H<sub>2</sub>O/Ce of the melt inclusions is  
421 quite constant (i.e., 197±58 2SD, N=15) over a range of <sup>87</sup>Sr/<sup>86</sup>Sr from 0.704858 to 0.709225,

422 and the melt inclusions with the strongest EM2 mantle signatures (i.e.,  $^{87}\text{Sr}/^{86}\text{Sr} > 0.7080$ , N=4)  
423 have elevated  $\text{H}_2\text{O}/\text{Ce}$  ( $193 \pm 19$  2SD) that is indistinguishable from the  $\text{H}_2\text{O}/\text{Ce}$  ( $202 \pm 31$ ) in melt  
424 inclusions with weaker EM2 signatures ( $^{87}\text{Sr}/^{86}\text{Sr} < 0.7080$ , N=3).

425 While the Samoan pillow glasses and melt inclusions exhibit some overlap with each other in  
426  $\text{H}_2\text{O}/\text{Ce}$  at the lowest  $^{87}\text{Sr}/^{86}\text{Sr}$ , they exhibit diverging trends in  $\text{H}_2\text{O}/\text{Ce}$  with increasing  $^{87}\text{Sr}/^{86}\text{Sr}$ :  
427 melt inclusions exhibit unchanging  $\text{H}_2\text{O}/\text{Ce}$  with increasing  $^{87}\text{Sr}/^{86}\text{Sr}$ , and glass exhibit  
428 decreasing  $\text{H}_2\text{O}/\text{Ce}$  with increasing  $^{87}\text{Sr}/^{86}\text{Sr}$ . Thus, the difference in  $\text{H}_2\text{O}/\text{Ce}$  between melt  
429 inclusions and glasses is largest at the highest  $^{87}\text{Sr}/^{86}\text{Sr}$  (Figure 7). To illustrate this, we note that  
430 all four pillow glasses with the strongest EM2 signatures ( $^{87}\text{Sr}/^{86}\text{Sr} > 0.7080$ ) have  $\text{H}_2\text{O}/\text{Ce} < 90$   
431 ( $\text{H}_2\text{O}/\text{Ce}$  average of  $75 \pm 30$ , 2SD) while the  $\text{H}_2\text{O}/\text{Ce}$  of the four melt inclusions with the highest  
432  $^{87}\text{Sr}/^{86}\text{Sr}$  ( $> 0.7080$ ) have  $\text{H}_2\text{O}/\text{Ce}$  that is more than twice as high as that in the pillow glasses  
433 ( $\text{H}_2\text{O}/\text{Ce}$  average of  $193 \pm 19$ , 2SD). Prior studies (e.g., Workman et al., 2006) often cite that  
434 pillow glasses erupted at depths  $> 1000$  mbsl retain volatile/ITE ratios of the mantle source. All  
435 pillow glasses shown in Figure 7 have  $\text{H}_2\text{O}-\text{CO}_2$  saturation pressures  $\geq 0.1$  kbar. Given that the  
436 melt inclusions and glasses in Figure 7 exhibit deep saturation pressures and appear to sample  
437 the same mantle source (Figure 4), we might expect the deeply-erupted pillow glasses should  
438 have the same  $\text{H}_2\text{O}/\text{Ce}$  as melt inclusions. These observations raise a key question that we will  
439 address in the discussion: why do melt inclusions and pillow glasses erupted at depths  $> 1000$   
440 mbsl from the same volcanoes and with the same  $^{87}\text{Sr}/^{86}\text{Sr}$  (i.e., sampling the same mantle  
441 sources) have  $\text{H}_2\text{O}/\text{Ce}$  that differ, on average, by nearly a factor of two?

442

## 443 **5. Modeling degassing processes for Samoan melts**

444 We find that melt inclusions from the Vailulu‘u and Malumalu seamounts have higher  
445 CO<sub>2</sub> concentrations than their corresponding pillow glasses (Figure 6), indicating that the deeply-  
446 erupted submarine pillow glasses are more degassed than the melt inclusions. An outstanding  
447 question is whether the lower H<sub>2</sub>O/Ce in the pillow glasses reflects this higher degree of  
448 degassing via concomitant degassing of both CO<sub>2</sub> and H<sub>2</sub>O.

449 We show that the data are consistent with Samoan pillow glasses being related to the  
450 Samoan melt inclusions through closed-system degassing; the new insight gained here is that,  
451 when compared with genetically-related melt inclusions, it is clear that even deeply erupted  
452 glasses (with CO<sub>2</sub>-H<sub>2</sub>O saturation pressures  $\geq 0.1$  kbar) have lost significant H<sub>2</sub>O and have lower  
453 H<sub>2</sub>O/Ce compared to their primary melt (Figure 3). This is evident in models we have run using a  
454 set of open- and closed-system degassing paths while also varying the fraction of CO<sub>2</sub>+H<sub>2</sub>O fluid  
455 in equilibrium with the initial melt (Figure 6). In the models, we define the variable M as the  
456 percentage of fluid in equilibrium with the melt, where M = 0% means that no initial fluid is in  
457 equilibrium with the melt (i.e., all volatiles are dissolved in the melt, no fluid is present), and  
458 where M = 100% means that all volatiles are in the fluid (i.e., no melt is present). The higher the  
459 M value, the deeper degassing starts. We generate degassing paths assuming a starting H<sub>2</sub>O and  
460 CO<sub>2</sub> composition equivalent to the melt inclusion with the highest H<sub>2</sub>O content from Malumalu  
461 seamount (sample AVON3-78-1#3) to model Malumalu data, and the equivalent high-H<sub>2</sub>O melt  
462 inclusion from Vailulu‘u (sample AVON3-71-2#10) to model Vailulu‘u data. We use MagmaSat  
463 (Ghiorso & Gualda, 2015) to calculate the fluid composition (i.e.,  $X_{\text{CO}_2}$  and  $X_{\text{H}_2\text{O}}$ ) in  
464 equilibrium with the two melt inclusions (see Table S9 for model melt inclusion compositions).  
465 Additionally, we use rhyolite-MELTS v.1.2 (which incorporates the same fluid solubility model  
466 as MagmaSat) to simulate degassing because this model is well-suited for high CO<sub>2</sub> contents in

467 the initial melt composition (Ghiorso & Gualda, 2015; Gualda et al., 2012). The models are run  
468 at 1200 °C, and start at 7–15 kbar (for Malumalu degassing paths, due to higher initial CO<sub>2</sub>  
469 contents), or 7 kbar (for Vailulu‘u, which has lower initial CO<sub>2</sub>), and run to 1 bar. The influence  
470 of oxygen fugacity on the model degassing path is negligible, so we assume QFM for all models.  
471 The compositional and physical parameters used in the MagmaSat and rhyolite-MELTS models  
472 are given in Table S9.

473 The degassing model results are presented in Figure 6. While there is no single degassing  
474 path that explains the difference in pillow glass and melt inclusion CO<sub>2</sub> and H<sub>2</sub>O concentrations,  
475 closed-system degassing paths with M values ranging from 0% to 10% describe most of the  
476 pillow glasses from both seamounts. However, there are some Vailulu‘u pillow glasses that have  
477 H<sub>2</sub>O that is higher than the range described by the calculated degassing paths. For example, three  
478 Vailulu‘u pillow glasses have higher H<sub>2</sub>O concentrations than the highest-H<sub>2</sub>O melt inclusion.  
479 This could be because the melt inclusion suite in this study does not represent the full range of  
480 H<sub>2</sub>O contents possible at the seamount, and higher initial H<sub>2</sub>O concentrations may be more  
481 reflective of the primary melts.

482 A primary observation from this modeling exercise is that closed-system degassing from  
483 melt inclusion entrapment pressures (i.e., >0.87 kbar) to eruption on the seafloor (pillow glasses  
484 have equilibrium pressures of 0.08 to 0.53 kbar) results in significant loss of both CO<sub>2</sub> and H<sub>2</sub>O,  
485 even for glasses with CO<sub>2</sub>-H<sub>2</sub>O saturation depths near 0.4 kbar (see closed-system degassing  
486 paths in Figure 6). Furthermore, the presence of equilibrium fluid (M) indicates that the  
487 magmatic system is richer in CO<sub>2</sub>, and thus starts to degas at greater depths. Below we show that  
488 loss of H<sub>2</sub>O during closed-system degassing to shallow levels (i.e., <0.53 kbar) explains the  
489 lower H<sub>2</sub>O/Ce in pillow glasses compared to the melt inclusions.

490 **6. Discussion**

491 H<sub>2</sub>O has incompatibility during mantle melting similar Ce (Michael, 1995), thus H<sub>2</sub>O/Ce  
492 of the melt inclusions and glasses should reflect the mantle source unless the samples have  
493 degassed. Clear negative correlations between H<sub>2</sub>O/Ce and <sup>87</sup>Sr/<sup>86</sup>Sr in pillow glasses have been  
494 used to infer the H<sub>2</sub>O/LREE (light rare earth element) ratios of the mantle source, assuming the  
495 H<sub>2</sub>O has not been degassed. The primary observation in this study that we seek to explain is that  
496 Samoan pillow glasses and olivine-hosted melt inclusions span the same range of <sup>87</sup>Sr/<sup>86</sup>Sr and  
497 trace element ratios—and thus sample the same mantle sources, yet the melt inclusions have  
498 H<sub>2</sub>O/Ce ratios that are approximately twice as high as the pillow glasses. The second key  
499 observation is that the melt inclusion H<sub>2</sub>O/Ce ratios are relatively constant over a wide range of  
500 <sup>87</sup>Sr/<sup>86</sup>Sr, in contrast to the pillow glasses whose H<sub>2</sub>O/Ce ratios anticorrelate with <sup>87</sup>Sr/<sup>86</sup>Sr. This  
501 raises two key questions: Why do Samoan EM2 pillow glasses exhibit H<sub>2</sub>O/Ce that are  
502 approximately half the values in Samoan EM2 melt inclusions at the same seamounts, and what  
503 does this mean for the H<sub>2</sub>O content of the EM2 mantle?

504

505 **6.1. Higher H<sub>2</sub>O/Ce in melt inclusions relative to pillow glasses: Diffusive H<sub>2</sub>O gain through**  
506 **host olivine and/or assimilation of seawater-derived materials?**

507 In order to compare the volatile contents of the Samoan melt inclusions and pillow  
508 glasses in this study, it is important to assess whether the higher H<sub>2</sub>O/Ce in the inclusions reflects  
509 processes operating in the magma during ascent, such as diffusive proton gain (i.e., addition of  
510 H) or assimilation of seawater-derived materials. Prior work has shown that, compared to large  
511 melt inclusions, small inclusions are more susceptible to diffusive loss or addition of protons,

512 and this results in modified  $\delta D$  (Hauri, 2002; Portnyagin et al., 2008; Gaetani et al., 2012;  
513 Bucholz et al., 2013; Hartley et al., 2015). Given enough time, the  $\delta D$  of all inclusions will  
514 eventually equilibrate with the external melt. Diffusive proton loss from the inclusion can be  
515 identified by an increase in  $\delta D$ , which is associated with decreasing melt inclusion volume.  
516 Conversely, diffusive gain of protons by the inclusion is identified by a decrease in  $\delta D$ , where  
517 the magnitude of the  $\delta D$  reduction is greater in the smaller volume melt inclusions. The new  $\delta D$   
518 analyses on melt inclusions show a lack of variation in  $\delta D$  ( $-35.8 \pm 17.0\%$ , 2SD, N=19) with melt  
519 inclusion size for melt inclusions with volumes  $>10^5 \mu\text{m}^3$ , which indicates no water loss or gain  
520 in the larger inclusions (Figure 2). However, the two smallest melt inclusions (AVON3-78-1#13  
521 and AVON3-78-1#32), both with melt inclusion volume  $<10^5 \mu\text{m}^3$ , have significantly higher  $\delta D$   
522 ( $+128\%$  and  $+6\%$ , respectively) than the other melt inclusions from this lava, which indicates  
523 that the small volume melt inclusions have experienced diffusive  $\text{H}_2\text{O}$  loss, not  $\text{H}_2\text{O}$  addition  
524 (Figure 2). These two small volume inclusions are excluded from the discussion below.

525         Assimilation of seawater-derived materials can increase  $\text{H}_2\text{O}$  in magmas (except if the  
526 magma is saturated in  $\text{H}_2\text{O}$ ), and this process can be traced by monitoring Cl/Nb, a ratio that is  
527 elevated in seawater-derived materials. One hypothesis for the higher  $\text{H}_2\text{O}/\text{Ce}$  in melt inclusions  
528 is that they have experienced more assimilation of seawater-derived materials compared to  
529 Samoan pillow glasses, and this hypothesis can be tested by measurement of  $^{87}\text{Sr}/^{86}\text{Sr}$ . A plot of  
530 Cl/Nb versus  $^{87}\text{Sr}/^{86}\text{Sr}$  shows that Samoan pillow glasses and melt inclusions have an  
531 overlapping range of Cl/Nb at any given  $^{87}\text{Sr}/^{86}\text{Sr}$ , so the offset to higher  $\text{H}_2\text{O}/\text{Ce}$  in the melt  
532 inclusions is not explained by greater assimilation experienced by melt inclusions (Figure 5). We  
533 do acknowledge that one melt inclusion with exceptionally high Cl/Nb (840)—a ratio consistent  
534 with assimilation of seawater-derived materials (Table S1)—also has elevated  $\text{H}_2\text{O}/\text{Ce}$  (366),



535 suggesting a role for assimilation in increasing the H<sub>2</sub>O/Ce in this particular inclusion. However,  
536 this single inclusion has been excluded from the discussion below owing to its very high Cl/Nb.

537 In short, diffusive gain of H<sub>2</sub>O and preferential assimilation of seawater-derived materials  
538 by the melt inclusions relative to the pillow glasses do not explain the higher H<sub>2</sub>O/Ce in the melt  
539 inclusions relative to the pillow glasses. Instead, we argue in the following section that closed-  
540 system degassing plays a key role in lowering the H<sub>2</sub>O and the H<sub>2</sub>O/Ce of pillow glasses. In  
541 contrast, limited H<sub>2</sub>O degassing has occurred in the melt inclusions in this study, leaving the melt  
542 inclusion H<sub>2</sub>O/Ce relatively unchanged, thereby explaining why melt inclusions have higher  
543 H<sub>2</sub>O/Ce than pillow glasses. This contrasts with prior studies (e.g., Workman et al., 2006)  
544 suggesting that pillow glasses erupted at depths >1000 mbsl retain H<sub>2</sub>O/LREE ratios of the  
545 mantle source.

546 **6.2 Higher H<sub>2</sub>O/Ce in melt inclusions relative to pillow glasses: H<sub>2</sub>O loss in Samoan glasses**  
547 **caused by degassing**

548 We argue that the difference in H<sub>2</sub>O/Ce between Samoan EM2-flavored melt inclusions  
549 and pillow glasses from the same seamounts relates to greater degassing of the pillow glasses  
550 relative to the melt inclusions. Unlike the pillow glasses, which can experience degassing from  
551 great depth all the way to eruption and quenching on the seafloor, melt inclusions trap melts at  
552 magma chamber depths and act as pressure vessels, which inhibits degassing at shallower levels  
553 during magma ascent. To evaluate this hypothesis, we build on the indistinguishable <sup>87</sup>Sr/<sup>86</sup>Sr  
554 and nonvolatile incompatible trace element ratios between pillow glasses and melt inclusions and  
555 argue that, at the depth of melt inclusion entrapment, the H<sub>2</sub>O/Ce of the melts that later erupted  
556 as Samoan pillow glasses was *also* the same as the Samoan melt inclusions (i.e., nonvolatile ITE  
557 ratios—which remain unmodified from primary melt compositions during fractional

558 crystallization of magmas with MgO as high as identified in the data reported here (Figure S1)—  
559 and  $^{87}\text{Sr}/^{86}\text{Sr}$  data obtained on the melt inclusions indicate that they derive from the same  
560 parental melts as the pillow glasses and thus should have started with the same  $\text{H}_2\text{O}/\text{Ce}$ . The  
561  $\text{H}_2\text{O}/\text{Ce}$  of the pillow glasses, but not the melt inclusions, was then lowered by  $\text{H}_2\text{O}$  degassing  
562 during ascent.

563         The hypothesis of  $\text{H}_2\text{O}$  loss from the matrix melts by degassing is supported by closed-  
564 system degassing models in Figure 6. For example, the degassing model for Malumalu AVON3-  
565 78-1 starts with a melt inclusion composition like AVON3-78-1#3 which has an elevated  $\text{CO}_2$   
566 concentration of 2810 ppm, the highest  $\text{H}_2\text{O}$  concentration from this lava (1.95 wt.%), and a high  
567 entrapment pressure of 2.63 kbar (i.e., the  $\text{CO}_2$ - $\text{H}_2\text{O}$  saturation pressure calculated for the melt  
568 inclusion using MagmaSat). Closed-system degassing of this melt composition from 2.63 kbar to  
569 0.2 kbar—the approximate  $\text{CO}_2$ - $\text{H}_2\text{O}$  saturation pressure for the pillow glass from this lava,  
570 sample AVON3-78-1—at  $M=1.6$  lowers the water content by a factor of  $\sim 2.1$  to 0.90 wt.%, and  
571 the  $\text{CO}_2$  content by a factor of  $\sim 40$  to 69 ppm. The red “x” in Figure 6a defines the  $\text{CO}_2$  and  $\text{H}_2\text{O}$   
572 composition of the model melt following degassing, and the degassed model melt is very similar  
573 in composition to the pillow glass sample AVON3-78-1 and helps explain the low  $\text{H}_2\text{O}$  (0.91  
574 wt.%) and  $\text{CO}_2$  (70 ppm) of AVON3-78-1. This is important because this particular pillow glass  
575 sample anchors the highest  $^{87}\text{Sr}/^{86}\text{Sr}$  (0.7089) and lowest  $\text{H}_2\text{O}/\text{Ce}$  (59) portion of the  $^{87}\text{Sr}/^{86}\text{Sr}$   
576 versus  $\text{H}_2\text{O}/\text{Ce}$  array produced by Workman et al. (2006) who interpreted that the low  $\text{H}_2\text{O}/\text{Ce}$  in  
577 this EM2 glass reflects melting of a water-poor (“dry”) EM2 mantle. In contrast, we show that  
578 dramatic  $\text{H}_2\text{O}$ -loss during closed-system degassing of an ascending EM2 melt with an initially  
579 high  $\text{H}_2\text{O}/\text{Ce}$  ratio ( $\text{H}_2\text{O}/\text{Ce} = 200$ ) is responsible for the low  $\text{H}_2\text{O}/\text{Ce}$  (59) in the AVON3-78-1  
580 glass. This model contrasts with prior studies (e.g., Workman et al., 2006) suggesting that pillow

581 glasses erupted at depths >1000 mbsl ( $\geq 0.1$  kbar) retain the H<sub>2</sub>O/LREE ratios of the mantle  
582 source.

583 We observe a relatively constant and elevated H<sub>2</sub>O/Ce ratio in melt inclusions over a  
584 wide range of <sup>87</sup>Sr/<sup>86</sup>Sr—melt inclusions with strong EM2 mantle signatures (i.e., <sup>87</sup>Sr/<sup>86</sup>Sr >  
585 0.7080) have elevated H<sub>2</sub>O/Ce (193±19 2SD, N=4) that is indistinguishable from H<sub>2</sub>O/Ce  
586 (202±31, N=3) in melt inclusions with weaker EM2 signatures (<sup>87</sup>Sr/<sup>86</sup>Sr < 0.7080). This also  
587 contrasts with Workman et al.'s (2006) observation that H<sub>2</sub>O/LREE is lower in the Samoan EM2  
588 pillow glasses with higher <sup>87</sup>Sr/<sup>86</sup>Sr. Unlike Workman et al. (2006), who argued that the low  
589 H<sub>2</sub>O/LREE in Samoan EM2 glasses is a source feature, we show that the low ratio in these  
590 pillow glasses relative to that of the melt inclusions can be explained by closed-system degassing  
591 of magmas during ascent to the seafloor. If this degassing model is correct, and if Samoan high  
592 <sup>87</sup>Sr/<sup>86</sup>Sr and low <sup>87</sup>Sr/<sup>86</sup>Sr melts have the same initial H<sub>2</sub>O/Ce—as supported by observations  
593 from melt inclusions in Figure 5a—then the negative correlation between <sup>87</sup>Sr/<sup>86</sup>Sr in H<sub>2</sub>O/Ce in  
594 the pillow glasses in Workman et al. (2006) (Figure 7) leads us to an important conclusion: the  
595 Samoan EM2 pillow glasses have degassed more H<sub>2</sub>O (to achieve lower H<sub>2</sub>O/Ce) than Samoan  
596 pillow glasses with weaker EM2 signatures (which have higher H<sub>2</sub>O/Ce). Therefore, we next  
597 focus on identifying the mechanism that results in greater H<sub>2</sub>O degassing in more extreme EM  
598 melts relative to non-EM melts.

599

600 **6.3 Explaining the inverse relationship between <sup>87</sup>Sr/<sup>86</sup>Sr and H<sub>2</sub>O/Ce in global pillow**  
601 **glasses by degassing.**

602 The global OIB dataset on submarine pillow glasses exhibits an inverse relationship  
603 between <sup>87</sup>Sr/<sup>86</sup>Sr and H<sub>2</sub>O/Ce (Figure 7) that is similar to the inverse correlation observed in

604 Samoan submarine glasses, and it has long been known that submarine glasses with low  $^{87}\text{Sr}/^{86}\text{Sr}$   
605 tend to have higher  $\text{H}_2\text{O}/\text{Ce}$  than glasses with high  $^{87}\text{Sr}/^{86}\text{Sr}$  (e.g., Dixon et al., 2002; Workman  
606 et al., 2006; Kendrick et al., 2014). The Samoan melt inclusions noticeably stray from this trend.  
607 The Samoan melt inclusions with high  $^{87}\text{Sr}/^{86}\text{Sr}$  are shifted to higher, relatively constant  $\text{H}_2\text{O}/\text{Ce}$   
608 ( $197\pm 58$  2SD,  $N=15$ ) compared to the  $\text{H}_2\text{O}/\text{Ce}$  ( $108\pm 58$ , 2SD,  $N=41$ ) in a global database of OIB  
609 glasses (including Samoa) that have similarly high  $^{87}\text{Sr}/^{86}\text{Sr}$  (i.e.,  $>0.7037$ ) (Figure 7). In fact, the  
610 high  $\text{H}_2\text{O}/\text{Ce}$  of Samoan inclusions ( $197\pm 58$  2SD,  $N=15$ ) is similar to the  $\text{H}_2\text{O}/\text{Ce}$  ( $209\pm 92$ , 2SD,  
611  $N=32$ ) of pillow glasses characterized by low  $^{87}\text{Sr}/^{86}\text{Sr}$  ( $<0.7037$ , the threshold value used to  
612 distinguish between EM and non-EM melts). If the Samoan melt inclusions represent less  
613 degassed versions of the melts sampled by Samoan submarine glasses, then the similarity in  
614  $\text{H}_2\text{O}/\text{Ce}$  between low  $^{87}\text{Sr}/^{86}\text{Sr}$  ( $<0.7037$ ) OIB pillow glasses and Samoan melt inclusions  
615 ( $>0.7037$ ) raises the possibility that non-EM OIB melts and EM OIB melts initially have the  
616 same  $\text{H}_2\text{O}/\text{Ce}$ , but the latter suffer more degassing of  $\text{H}_2\text{O}$  than the former during magma ascent.  
617 If the inverse correlation between  $\text{H}_2\text{O}/\text{Ce}$  and  $^{87}\text{Sr}/^{86}\text{Sr}$  in Samoan, and global, OIB glasses is  
618 driven by greater degassing of the most geochemically enriched lavas compared to  
619 geochemically depleted lavas, what mechanism causes geochemically enriched glasses from OIB  
620 mantle sources to have suffered more  $\text{H}_2\text{O}$  degassing than geochemically depleted glasses?

621 Previous work suggests that EM mantle sources have higher  $\text{CO}_2$ , and generate primary  
622 melts with higher  $\text{CO}_2$ , than non-EM mantle sources (Burnard et al., 2014; Cartigny et al., 2008;  
623 Taracsák et al., 2019; Hauri et al., 2018; Miller et al 2019; Matthews et al. 2021; Michael &  
624 Graham, 2015; Shimizu et al., 2023). We show that primary melts with higher  $\text{CO}_2$  degas more  
625  $\text{CO}_2$  and more  $\text{H}_2\text{O}$  by closed-system degassing during ascent than primary melts with the same  
626  $\text{H}_2\text{O}$  but lower  $\text{CO}_2$  concentrations. As a result, EM lavas that were initially more  $\text{CO}_2$ -rich erupt

627 on the seafloor with lower H<sub>2</sub>O/Ce than their geochemically-depleted non-EM counterparts that  
628 started with lower primary melt CO<sub>2</sub>, even though both EM and non-EM primary melts started  
629 with the same H<sub>2</sub>O concentrations and H<sub>2</sub>O/Ce. At the extreme end, non-EM (i.e., geochemically  
630 depleted) melts erupted at, for example, MORB settings, can have such low primary melt CO<sub>2</sub>  
631 that they never saturate and neither CO<sub>2</sub> nor H<sub>2</sub>O are lost by degassing (Saal et al., 2002;  
632 Michael & Graham, 2015; Hauri et al., 2018).

633 By contrast, we argue that CO<sub>2</sub>-rich primary melts, typical of geochemically-enriched  
634 OIB settings, saturate CO<sub>2</sub> at great depths and lose significant CO<sub>2</sub> and H<sub>2</sub>O by closed-system  
635 degassing. In order to show this, we first estimate primary melt CO<sub>2</sub> for a suite of global OIB  
636 glasses using a set of relationships shown in Figures 8 and 9. Because OIB glasses are degassed  
637 in CO<sub>2</sub> to variable degrees, we estimate primary melt (undegassed) CO<sub>2</sub> for OIB glasses in the  
638 following way. First, using a new correlation between undegassed CO<sub>2</sub>/Nb and (La/Sm)<sub>N</sub> in  
639 MORB and OIB (see equation in Figure 9a and discussion in Supplementary Information section  
640 S1.8), together with the measured (La/Sm)<sub>N</sub> available in the suite of OIB glasses examined here,  
641 we can calculate the primary melt CO<sub>2</sub>/Nb in the OIB glasses (Figure 8c). (It is worth noting that  
642 the correlation between CO<sub>2</sub>/Nb and (La/Sm)<sub>N</sub> in Figure 9a is similar to a relationship previously  
643 suggested for MORB by Cartigny et al. (2008) (Figure 9b).) We then calculate the primary melt  
644 Nb concentrations for each of the OIB glasses by correcting for olivine addition or subtraction so  
645 the melts are in equilibrium with mantle (F<sub>090</sub>) olivine (Figure 8d). By multiplying calculated  
646 primary melt CO<sub>2</sub>/Nb (Figure 8c) by the calculated primary melt Nb concentrations (Figure 8d),  
647 we obtain primary melt CO<sub>2</sub> concentrations for the OIB glasses (Figure 8e). These calculations  
648 suggest that the most extreme EM OIB glasses (which have the lowest H<sub>2</sub>O/Ce)—all from the  
649 Samoa, Societies, and Pitcairn hotspots—tend to have the highest primary melt CO<sub>2</sub> (Figure 8e),

650 with CO<sub>2</sub> concentrations commonly as high as 5 to 6 wt.% in Samoa and Societies lavas (and  
651 higher than 80,000 ppm CO<sub>2</sub> in two Samoan lavas). These high OIB primary melt CO<sub>2</sub>  
652 concentrations calculated with our new model are in broad agreement with CO<sub>2</sub> concentrations  
653 calculated using the petrologic model of Sun and Dasgupta (2020) (see supplementary Figure S9  
654 for direct comparison).

655         Based on these calculations, Samoan primary melts inferred from the pillow rim glass  
656 data have CO<sub>2</sub> concentrations between ~28,000 ppm and ~94,000 ppm, with most values  
657 clustering near ~60,000 ppm CO<sub>2</sub> (Figure 8e). With few exceptions, the non-EM OIB (which  
658 have the highest erupted H<sub>2</sub>O/Ce)—Lō‘ihi, Easter, and Foundation—have lower calculated  
659 primary melt CO<sub>2</sub> than the EM OIB—Samoa, Societies, Pitcairn, and Réunion (Figure 8e). This  
660 is consistent with prior suggestions that geochemically enriched mantle domains with higher  
661 <sup>87</sup>Sr/<sup>86</sup>Sr generate primary melts with higher CO<sub>2</sub> than geochemically depleted mantle domains  
662 (Burnard et al., 2014; Cartigny et al., 2008). Like Burnard et al. (2014), we argue that melts with  
663 higher initial CO<sub>2</sub>—characteristic of EM melts (Figure 8e)—undergo greater degrees of  
664 degassing than melts with lower initial CO<sub>2</sub>. We then show that, everything else being the same,  
665 higher initial CO<sub>2</sub> melts experience greater degassing of H<sub>2</sub>O (and thus have lower erupted  
666 H<sub>2</sub>O/Ce) than melts with lower initial CO<sub>2</sub> (Figure 8).

667         In order to demonstrate this quantitatively, we use the calculated primary melt CO<sub>2</sub> of the  
668 OIB glasses in Figure 8e, as well as estimated primary melt H<sub>2</sub>O (see below), as inputs to a  
669 closed-system degassing model. We then show that the CO<sub>2</sub>-rich (60,000 ppm) model primary  
670 melt degasses by closed-system degassing to have H<sub>2</sub>O concentration and H<sub>2</sub>O/Ce similar to  
671 values measured in Samoan EM pillow glasses. To test our hypothesis that high primary melt  
672 CO<sub>2</sub> concentrations results in more degassing of H<sub>2</sub>O, and thus, lower H<sub>2</sub>O/Ce in the final

673 erupted and degassed melt, we examine how H<sub>2</sub>O and CO<sub>2</sub> concentrations change with  
674 decreasing pressure starting with two hypothetical primary melts that are identical in all respects  
675 except for the initial CO<sub>2</sub> concentrations: the two melt endmembers are given the same starting  
676 H<sub>2</sub>O (2 wt.%), H<sub>2</sub>O/Ce (200), and major and trace element chemistry (see compositions in Table  
677 S9). The first model melt is assigned a higher CO<sub>2</sub> concentration of 60,000 ppm, meant to  
678 approximate the elevated CO<sub>2</sub> concentration of EM glasses in Figure 8e (see previous  
679 paragraph), and comes from our new model for calculating CO<sub>2</sub> in OIB primary melts (Figure  
680 8c, 9a) for which calculated Samoan primary melt CO<sub>2</sub> concentrations tend to cluster near 60,000  
681 ppm CO<sub>2</sub>. The second model melt is assigned an initial CO<sub>2</sub> concentration of 5,000 ppm, and is  
682 meant to approximate the CO<sub>2</sub> concentration of the non-EM glasses from Foundation, Easter,  
683 and Lō‘ihi in Figure 8e. In order to illustrate the impact of H<sub>2</sub>O loss during degassing as a  
684 function of initial primary melt CO<sub>2</sub> concentration, we model the closed-system degassing paths  
685 of the two melts using rhyolite-MELTS. Degassing of the high CO<sub>2</sub> (60,000 ppm) melt starts at  
686 26 kbar (i.e., where CO<sub>2</sub> first saturates; see dark green line in Figure 10), which is higher than the  
687 4 kbar pressure where the lower CO<sub>2</sub> melt saturates (see light green line in Figure 10). After both  
688 the high- and low-CO<sub>2</sub> melts degas to the same low eruptive pressure (Figure 10)—0.5 kbar,  
689 meant to represent pressure for eruption on the seafloor at ~5000 mbsl—the high CO<sub>2</sub> melt has a  
690 significantly lower H<sub>2</sub>O concentration and lower H<sub>2</sub>O/Ce (~0.94 wt.% and 94, respectively)  
691 compared to the low CO<sub>2</sub> melt (~1.56 wt.% wt.% and 156, respectively), even though both melts  
692 started with the same H<sub>2</sub>O (2 wt.%) and H<sub>2</sub>O/Ce (200). In summary, a melt with initial CO<sub>2</sub> of  
693 60,000 ppm degases nearly 53% of its H<sub>2</sub>O (and 99.4% of its CO<sub>2</sub>) during ascent to 0.5 kbar, but  
694 the melt with 5000 ppm initial CO<sub>2</sub> degases just 22% of its H<sub>2</sub>O (and 96.8% of its CO<sub>2</sub>) during

695 ascent to 0.5 kbar. Thus, everything else being the same, high CO<sub>2</sub> melts degas more H<sub>2</sub>O and  
696 have lower H<sub>2</sub>O/Ce than low CO<sub>2</sub> melts.

697         The simple degassing model in Figure 10 helps explain the observation that EM pillow  
698 glasses erupted on the seafloor have lower H<sub>2</sub>O/Ce compared to non-EM pillow glasses: EM  
699 primary melts, which are associated with higher initial CO<sub>2</sub> (Figure 8e), saturate in volatiles  
700 deeper in the crust/mantle and degas more CO<sub>2</sub> and H<sub>2</sub>O prior to eruption than non-EM melts  
701 with lower primary melt CO<sub>2</sub>. The Samoan melt inclusions in this study exhibit high H<sub>2</sub>O/Ce,  
702 similar to non-EM melts, because CO<sub>2</sub> and H<sub>2</sub>O degassing was arrested following melt inclusion  
703 entrapment in olivine at high pressures (0.870 to 5.13 kbar). Although the Samoan melt  
704 inclusions lost significant amounts of CO<sub>2</sub> prior to being entrapped by olivine, these melt  
705 inclusions still preserve higher H<sub>2</sub>O/Ce than the erupted pillow glasses due to having degassed  
706 less CO<sub>2</sub> and, thus, less H<sub>2</sub>O. However, we acknowledge that, prior to entrapment, even the melt  
707 inclusions may have already lost some H<sub>2</sub>O due to concomitant loss of both H<sub>2</sub>O and CO<sub>2</sub> during  
708 closed-system degassing. Nonetheless, melt inclusions preserve higher H<sub>2</sub>O and H<sub>2</sub>O/Ce than  
709 pillow glasses, and thus preserve values closer to the primary melts.

710 **6.4 Comparison with prior models for the origin of low H<sub>2</sub>O/Ce in EM lavas, and**  
711 **implications for a “damp” EM mantle.**

712         Previous studies have suggested that the negative correlation between H<sub>2</sub>O/Ce and  
713 <sup>87</sup>Sr/<sup>86</sup>Sr is the result of dehydration (H<sub>2</sub>O depletion) in the EM source, which has low H<sub>2</sub>O/Ce  
714 that gives rise to EM primary melts with low H<sub>2</sub>O/Ce. In these models, the EM mantle source  
715 has low H<sub>2</sub>O/Ce because subducted materials contributing to the EM mantle lose H<sub>2</sub>O during  
716 subduction (Dixon et al., 2002) or via diffusion during residence in the mantle (Workman et al.,  
717 2006), or because the pyroxenite—which has low H<sub>2</sub>O/Ce—contributes to the EM mantle



718 (Bizimis & Peslier et al., 2015). However, if these models explained the origin of the low  
719 H<sub>2</sub>O/Ce in high <sup>87</sup>Sr/<sup>86</sup>Sr glasses from Samoa, then the Samoan melt inclusions with high  
720 <sup>87</sup>Sr/<sup>86</sup>Sr should also exhibit lower H<sub>2</sub>O/Ce, but this is not the case.

721 Thus, an important implication is that submarine glasses cannot be reliably used to  
722 estimate the H<sub>2</sub>O/Ce content of OIB primary melts, particularly glasses for EM OIB that appear  
723 to experience greater degassing (owing to higher initial CO<sub>2</sub>) than non-EM OIB. Our data show  
724 that, unlike Samoan submarine glasses, Samoan melt inclusions have similar H<sub>2</sub>O/Ce (197±58,  
725 2SD, N=15) that does not vary with <sup>87</sup>Sr/<sup>86</sup>Sr. In fact, the H<sub>2</sub>O/Ce ratio (193±19, 2SD, N=4) for  
726 extreme Samoan EM2 (<sup>87</sup>Sr/<sup>86</sup>Sr > 0.708) melt inclusions overlaps with H<sub>2</sub>O/Ce suggested for  
727 depleted mantle domains that are sampled by non-EM OIB (<sup>87</sup>Sr/<sup>86</sup>Sr < 0.7037; H<sub>2</sub>O/Ce =  
728 209±92), average Pacific MORB (180±20; Dixon et al., 2017), average depleted N. Atlantic  
729 MORB (230±20; Dixon et al., 2017), and PREMA (*Prevalent Mantle*) Pacific and Atlantic OIB  
730 (215±30 and 220±30, respectively, where PREMA-type OIB do not bear EM or HIMU  
731 signatures; Dixon et al., 2017). Thus, the major implication of this work is that, instead of being  
732 “dry”, the EM2 mantle sampled by Samoa is just as “damp” as non-EM reservoirs, but this can  
733 only be seen by examining deeply entrapped melt inclusions that preserve higher CO<sub>2</sub> and H<sub>2</sub>O  
734 than submarine pillow glasses. Due to pronounced CO<sub>2</sub> and concomitant H<sub>2</sub>O degassing that  
735 appears to impact enriched lavas more than depleted ones—owing to higher primary melt CO<sub>2</sub> in  
736 the former relative to the latter—future melt inclusion studies will be important for determining  
737 the initial H<sub>2</sub>O/Ce in EM1 (Pitcairn) and other EM2 (Societies) lavas, where existing low  
738 H<sub>2</sub>O/Ce values measured in high <sup>87</sup>Sr/<sup>86</sup>Sr Pitcairn and Societies submarine glasses (Kendrick et  
739 al. 2014) may also be due to the same degassing mechanism that lowers H<sub>2</sub>O/Ce in Samoan OIB.  
740 If so, H<sub>2</sub>O/Ce in the mantle is not likely to be as variable as previously supposed, and much of

741 the mantle sampled by MORB and OIB have very similar H<sub>2</sub>O/Ce that is, on average, close to a  
742 value of 200, and not as low as values found in pillow glasses of EM lavas (down to 59 in  
743 Samoan pillow glasses, 86 in Societies glasses, and 95 in Pitcairn glasses). Thus, like the Pb/Ce  
744 ratio, which is similar in OIB and MORB globally (Hofmann et al., 1986), the H<sub>2</sub>O/Ce ratio may  
745 also be similar in the sources of plume-derived lavas (Michael, 1995).

746 A second implication of “damp” H<sub>2</sub>O/Ce in EM Samoan lavas is that, in spite of hosting  
747 subducted continental materials which have presumably lost H<sub>2</sub>O by degassing at an ancient  
748 subduction zone (White & Hofmann, 1982; Farley et al., 1992; Jackson et al., 2007), Samoan  
749 EM2 melt (as sampled by EM melt inclusions) do not have lower H<sub>2</sub>O/Ce than non-EM OIBs.  
750 This is a surprising result, and suggests that recycled continental materials may not play a large  
751 role in governing the H<sub>2</sub>O budgets of mantle domains. This could be because the amount of  
752 recycled continental crust in the mantle sources of OIB is small, and thus has a diminished  
753 impact on the overall H<sub>2</sub>O and H<sub>2</sub>O/Ce of the mantle source. For example, Samoan lava  
754 AVON3-78-1 examined in this study, which has a strong EM2 signature (<sup>87</sup>Sr/<sup>86</sup>Sr of 0.7089), is  
755 estimated to have only ~1% continental crust (Reinhard et al., 2018) that is added to a depleted  
756 plume component that constitutes the rest (99%) of the mantle source. In this model, the H<sub>2</sub>O and  
757 Ce budgets of the EM2 mantle source is primarily controlled by the depleted plume component,  
758 even if the recycled continental crust component has low H<sub>2</sub>O/Ce. In this way, both depleted  
759 mantle and EM OIB can have similar H<sub>2</sub>O/Ce.

760

761 **Acknowledgements:** MGJ gratefully acknowledges being wrong (and that John Lassiter was  
762 correct) in the debate about whether mantle source H<sub>2</sub>O/Ce is preserved in deeply dredged  
763 (>1000 mbsl) submarine pillow glasses. OEA thanks Marc Hirschmann for a discussion about

764 CO<sub>2</sub>/Nb in oceanic lavas, Gareth Seward for his skillful assistance with UCSB's electron  
765 microprobe, Jean-Luc Devidal for assisting EFR-K with LA-ICP-MS analyses, and Brian  
766 Monteleone for his time and help with ion probe analyses. MGJ acknowledges NSF grants OCE-  
767 1736984, EAR-1900652, OCE-1912931, and OCE-1929095 that supported this work.

768

## 769 **References cited**

- 770 Adams, J.V., Spera, F.J. and Jackson, M.G. (2021). Trachytic melt inclusions hosted in clinopyroxene  
771 offer a glimpse into Samoan EM2-endmember melts. *Geochemistry, Geophysics, Geosystems*, 22(3),  
772 p.e2020GC009212. <https://doi.org/10.1029/2020GC009212>
- 773 Anderson, A.T. (1974). Evidence for a picritic, volatile-rich magma beneath Mt. Shasta, California.  
774 *Journal of Petrology*, 15, 243–267. <https://doi.org/10.1093/petrology/15.2.243>
- 775 Anderson, K. R., & Poland, M. P. (2017). Abundant carbon in the mantle beneath Hawai'i. *Nature*  
776 *Geoscience*, 10(9), 704–708. <https://doi.org/10.1038/ngeo3007>
- 777 Anderson, O.E., Jackson, M.G., Rose-Koga, E.F., Marske, J.P., Peterson, M.E., Price, A.A., Byerly, B.L.  
778 and Reinhard, A.A. (2021). Testing the recycled gabbro hypothesis for the origin of “ghost plagioclase”  
779 melt signatures using <sup>87</sup>Sr/<sup>86</sup>Sr of individual olivine-hosted melt inclusions from Hawai'i. *Geochemistry,*  
780 *Geophysics, Geosystems*, 22(4). <https://doi.org/10.1029/2020GC009260>
- 781 Aiuppa, A., Casetta, F., Coltorti, M., Stagno, V., & Tamburello, G. (2021). Carbon concentration  
782 increases with depth of melting in Earth's upper mantle. *Nature Geoscience*, 14(9), 697–703.  
783 <https://doi.org/10.1038/s41561-021-00797-y>
- 784 Asimow, P. D., & Langmuir, A. C. (2003). The importance of water to oceanic mantle melting  
785 regimes. *Nature*, 421(6925), 815–820. <https://doi.org/10.1038/nature01429>
- 786 Aster, E. M., Wallace, P. J., Moore, L. R., Watkins, J., Gazel, E., & Bodnar, R. J. (2016). Reconstructing  
787 CO<sub>2</sub> concentrations in basaltic melt inclusions using Raman analysis of vapor bubbles. *Journal of*  
788 *Volcanology and Geothermal Research*, 323, 148–162. <https://doi.org/10.1016/j.jvolgeores.2016.04.028>
- 789 Aubaud, C. (2022). Carbon stable isotope constraints on CO<sub>2</sub> degassing models of ridge, hotspot and arc  
790 magmas. *Chemical Geology*, 605, 120962. <https://doi.org/10.1016/j.chemgeo.2022.120962>
- 791 Bizimis, M., & Peslier, A. H. (2015). Water in Hawaiian garnet pyroxenites: Implications for water  
792 heterogeneity in the mantle. *Chemical Geology*, 397, 61–75.  
793 <https://doi.org/10.1016/j.chemgeo.2015.01.008>
- 794 Boudoire, G., Rizzo, A. L., Di Muro, A., Grassa, F., & Liuzzo, M. (2018). Extensive CO<sub>2</sub> degassing in the  
795 upper mantle beneath oceanic basaltic volcanoes: First insights from Piton de la Fournaise volcano (La

- 796 Réunion Island). *Geochimica et Cosmochimica Acta*, 235, 376–401.  
 797 <https://doi.org/10.1016/j.gca.2018.06.004>
- 798 Bucholz, C. E., Gaetani, G. A., Behn, M. D., & Shimizu, N. (2013). Post-entrapment modification of  
 799 volatiles and oxygen fugacity in olivine-hosted melt inclusions. *Earth and Planetary Science Letters*, 374,  
 800 145–155. <https://doi.org/10.1016/j.epsl.2013.05.033>
- 801 Burnard, P., Reisberg, L., & Colin, A. (2014). An observed link between lithophile compositions and  
 802 degassing of volatiles (He, Ar, CO<sub>2</sub>) in MORBs with implications for Re volatility and the mantle C/Nb  
 803 ratio. *Earth and Planetary Science Letters*, 395, 159–167. <https://doi.org/10.1016/j.epsl.2014.03.045>
- 804 Cabral, R.A., Jackson, M.G., Koga, K.T., Rose-Koga, E.F., Hauri, E.H., Whitehouse, M.J., Price, A.A.,  
 805 Day, J.M., Shimizu, N. and Kelley, K.A., 2014. Volatile cycling of H<sub>2</sub>O, CO<sub>2</sub>, F, and Cl in the HIMU  
 806 mantle: A new window provided by melt inclusions from oceanic hot spot lavas at Mangaia, Cook  
 807 Islands. *Geochemistry, Geophysics, Geosystems*, 15(11), 4445–4467.  
 808 <https://doi.org/10.1002/2014GC005473>
- 809 Cartigny, P., Pineau, F., Aubaud, C., & Javoy, M. (2008). Towards a consistent mantle carbon flux  
 810 estimate: Insights from volatile systematics (H<sub>2</sub>O/Ce, δD, CO<sub>2</sub>/Nb) in the North Atlantic mantle (14 N  
 811 and 34 N). *Earth and Planetary Science Letters*, 265(3–4), 672–685.  
 812 <https://doi.org/10.1016/j.epsl.2007.11.011>
- 813 Danyushevsky, L. V., Della-Pasqua, F. N., & Sokolov, S. (2000). Re-equilibration of melt inclusions  
 814 trapped by magnesian olivine phenocrysts from subduction-related magmas: petrological implications.  
 815 *Contributions to Mineralogy and Petrology*, 138(1), 68–83. <https://doi.org/10.1007/PL00007664>
- 816 Danyushevsky, L. V., Leslie, R. A., Crawford, A. J., & Durance, P. (2004). Melt inclusions in primitive  
 817 olivine phenocrysts: the role of localized reaction processes in the origin of anomalous compositions.  
 818 *Journal of Petrology*, 45(12), 2531–2553. <https://doi.org/10.1093/petrology/egh080>
- 819 Danyushevsky, L. V., Perfit, M. R., Eggins, S. M., & Falloon, T. J. (2003). Crustal origin for coupled  
 820 'ultra-depleted' and 'plagioclase' signatures in MORB olivine-hosted melt inclusions: evidence from the  
 821 Siqueiros Transform Fault, East Pacific Rise. *Contributions to Mineralogy and Petrology*, 144(5), 619–  
 822 637. <https://doi.org/10.1007/s00410-002-0420-3>
- 823 Devey, C. W., Albarede, F., Cheminée, J. L., Michard, A., Mühe, R., & Stoffers, P. (1990). Active  
 824 submarine volcanism on the Society hotspot swell (West Pacific): a geochemical study. *Journal of*  
 825 *Geophysical Research: Solid Earth*, 95(B4), 5049–5066. <https://doi.org/10.1029/JB095iB04p05049>
- 826 DeVitre, C. L., Allison, C. M., & Gazel, E. (2021). A high-precision CO<sub>2</sub> densimeter for Raman  
 827 spectroscopy using a Fluid Density Calibration Apparatus. *Chemical Geology*, 584, 120522.  
 828 <https://doi.org/10.1016/j.chemgeo.2021.120522>
- 829 Dixon, J.E., Bindeman, I.N., Kingsley, R.H., Simons, K.K., Le Roux, P.J., Hajewski, T.R., Swart, P.,  
 830 Langmuir, C.H., Ryan, J.G., Walowski, K.J., & Wada, I. (2017). Light stable isotopic compositions of

- 831 enriched mantle sources: Resolving the dehydration paradox. *Geochemistry, Geophysics,*  
 832 *Geosystems*, 18(11), 3801–3839. <https://doi.org/10.1002/2016GC006743>
- 833 Dixon, J. E., & Clague, D. A. (2001). Volatiles in basaltic glasses from Loihi Seamount, Hawaii:  
 834 Evidence for a relatively dry plume component. *Journal of Petrology*, 42(3), 627–654.  
 835 <https://doi.org/10.1093/petrology/42.3.627>
- 836 Dixon, J. E., Clague, D. A., Wallace, P., & Poreda, R. (1997). Volatiles in alkalic basalts from the North  
 837 Arch Volcanic Field, Hawaii: extensive degassing of deep submarine-erupted alkalic series lavas. *Journal*  
 838 *of Petrology*, 38(7), 911–939. <https://doi.org/10.1093/petroj/38.7.911>
- 839 Dixon, J. E., Leist, L., Langmuir, C., & Schilling, J. G. (2002). Recycled dehydrated lithosphere observed  
 840 in plume-influenced mid-ocean-ridge basalt. *Nature*, 420(6914), 385–389.  
 841 <https://doi.org/10.1038/nature01215>
- 842 Farley, K. A., Natland, J. H., & Craig, H. (1992). Binary mixing of enriched and undegassed (primitive?)  
 843 mantle components (He, Sr, Nd, Pb) in Samoan lavas. *Earth and Planetary Science Letters*, 111(1), 183–  
 844 199. [https://doi.org/10.1016/0012-821X\(92\)90178-X](https://doi.org/10.1016/0012-821X(92)90178-X)
- 845 Ford, C. E., Russell, D. G., Craven, J. A., & Fisk, M. R. (1983). Olivine-liquid equilibria: temperature,  
 846 pressure and composition dependence of the crystal/liquid cation partition coefficients for Mg, Fe<sup>2+</sup>, Ca  
 847 and Mn. *Journal of Petrology*, 24(3), 256–266. <https://doi.org/10.1093/petrology/24.3.256>
- 848 Fortin, M. A., Riddle, J., Desjardins-Langlais, Y., & Baker, D. R. (2015). The effect of water on the  
 849 sulfur concentration at sulfide saturation (SCSS) in natural melts. *Geochimica et Cosmochimica Acta*,  
 850 160, 100–116. <https://doi.org/10.1016/j.gca.2015.03.022>
- 851 Fretzdorff, S., & Haase, K. M. (2002). Geochemistry and petrology of lavas from the submarine flanks of  
 852 Réunion Island (western Indian Ocean): implications for magma genesis and the mantle source.  
 853 *Mineralogy and Petrology*, 75, 153–184. <https://doi.org/10.1007/s007100200022>
- 854 Frey, F. A., Clague, D., Mahoney, J. J., & Sinton, J. M. (2000). Volcanism at the edge of the Hawaiian  
 855 plume: petrogenesis of submarine alkalic lavas from the North Arch volcanic field. *Journal of*  
 856 *Petrology*, 41(5), 667–691. <https://doi.org/10.1093/petrology/41.5.667>
- 857 Frezzotti, M. L. (2001). Silicate-melt inclusions in magmatic rocks: applications to petrology. *Lithos*,  
 858 55(1–4), 273–299. [https://doi.org/10.1016/S0024-4937\(00\)00048-7](https://doi.org/10.1016/S0024-4937(00)00048-7)
- 859 Gaetani, G. A., & Grove, T. L. (1998). The influence of water on melting of mantle  
 860 peridotite. *Contributions to Mineralogy and Petrology*, 131, 323–346.  
 861 <https://doi.org/10.1007/s004100050396>
- 862 Gaetani, G. A., O’Leary, J. A., Shimizu, N., Bucholz, C. E., & Newville, M. (2012). Rapid reequilibration  
 863 of H<sub>2</sub>O and oxygen fugacity in olivine-hosted melt inclusions. *Geology*, 40(10), 915–918.  
 864 <https://doi.org/10.1130/G32992.1>

- 865 Ghiorso, M. S., & Gualda, G. A. (2015). An H<sub>2</sub>O–CO<sub>2</sub> mixed fluid saturation model compatible with  
 866 rhyolite-MELTS. *Contributions to Mineralogy and Petrology*, 169, 1–30. <https://doi.org/10.1007/s00410->  
 867 015-1141-8
- 868 Graham, D. W., & Michael, P. J. (2021). Predominantly recycled carbon in Earth's upper mantle revealed  
 869 by He–CO<sub>2</sub>–Ba systematics in ultradepleted ocean ridge basalts. *Earth and Planetary Science Letters*, 554,  
 870 116646. <https://doi.org/10.1016/j.epsl.2020.116646>
- 871 Gualda G.A.R., Ghiorso M.S., Lemons R.V., Carley T.L. (2012) Rhyolite-MELTS: A modified  
 872 calibration of MELTS optimized for silica-rich, fluid-bearing magmatic systems. *Journal of Petrology*,  
 873 53, 875–890. <https://doi.org/10.1093/petrology/egr080>
- 874 Hanyu, T., Yamamoto, J., Kimoto, K., Shimizu, K., & Ushikubo, T. (2020). Determination of total CO<sub>2</sub> in  
 875 melt inclusions with shrinkage bubbles. *Chemical Geology*, 557, 119855.  
 876 <https://doi.org/10.1016/j.chemgeo.2020.119855>
- 877 Hartley, M. E., MacLennan, J., Edmonds, M., & Thordarson, T. (2014). Reconstructing the deep CO<sub>2</sub>  
 878 degassing behaviour of large basaltic fissure eruptions. *Earth and Planetary Science Letters*, 393, 120–  
 879 131. <https://doi.org/10.1016/j.epsl.2014.02.031>
- 880 Hartley, M. E., Neave, D. A., MacLennan, J., Edmonds, M., & Thordarson, T. (2015). Diffusive over-  
 881 hydration of olivine-hosted melt inclusions. *Earth and Planetary Science Letters*, 425, 168–178.  
 882 <https://doi.org/10.1016/j.epsl.2015.06.008>
- 883 Hauri, E. H. (1996). Major-element variability in the Hawaiian mantle plume. *Nature*, 382(6590), 415–  
 884 419. <https://doi.org/10.1038/382415a0>
- 885 Hauri, E. H., & Hart, S. R. (1993). ReOs isotope systematics of HIMU and EMII oceanic island basalts  
 886 from the south Pacific Ocean. *Earth and Planetary Science Letters*, 114(2–3), 353–371.  
 887 [https://doi.org/10.1016/0012-821X\(93\)90036-9](https://doi.org/10.1016/0012-821X(93)90036-9)
- 888 Hauri, E. (2002). SIMS analysis of volatiles in silicate glasses, 2: isotopes and abundances in Hawaiian  
 889 melt inclusions. *Chemical Geology*, 183(1–4), 115–141. [https://doi.org/10.1016/S0009-2541\(01\)00374-6](https://doi.org/10.1016/S0009-2541(01)00374-6)
- 890 Hauri, E. H., MacLennan, J., McKenzie, D., Gronvold, K., Oskarsson, N., & Shimizu, N. (2018). CO<sub>2</sub>  
 891 content beneath northern Iceland and the variability of mantle carbon. *Geology*, 46(1), 55–58.  
 892 <https://doi.org/10.1130/G39413.1>
- 893 Hirschmann, M. M. (2006). Water, melting, and the deep Earth H<sub>2</sub>O cycle. *Annu. Rev. Earth Planet.*  
 894 *Sci.*, 34, 629–653. <https://doi.org/10.1146/annurev.earth.34.031405.125211>
- 895 Hirschmann, M. M. (2018). Comparative deep Earth volatile cycles: The case for C recycling from  
 896 exosphere/mantle fractionation of major (H<sub>2</sub>O, C, N) volatiles and from H<sub>2</sub>O/Ce, CO<sub>2</sub>/Ba, and CO<sub>2</sub>/Nb  
 897 exosphere ratios. *Earth and Planetary Science Letters*, 502, 262–273.  
 898 <https://doi.org/10.1016/j.epsl.2018.08.023>
- 899 Hirth, G., & Kohlstedt, D. L. (1996). Water in the oceanic upper mantle: implications for rheology, melt  
 900 extraction and the evolution of the lithosphere. *Earth and Planetary Science Letters*, 144(1-2), 93-108.  
 901 [https://doi.org/10.1016/0012-821X\(96\)00154-9](https://doi.org/10.1016/0012-821X(96)00154-9)

- 902 Hirth, G., & Kohlstedt, D. (2003). Rheology of the upper mantle and the mantle wedge: A view from the  
 903 experimentalists. *Geophysical Monograph-American Geophysical Union*, 138, 83–106.  
 904 <https://doi.org/10.1029/138GM06>
- 905 Hofmann, A. W., Jochum, K. P., Seufert, M., & White, W. M. (1986). Nb and Pb in oceanic basalts: new  
 906 constraints on mantle evolution. *Earth and Planetary Science Letters*, 79(1–2), 33–45.  
 907 [https://doi.org/10.1016/0012-821X\(86\)90038-5](https://doi.org/10.1016/0012-821X(86)90038-5)
- 908 Iacovino, K., Matthews, S., Wieser, P. E., Moore, G. M., & Bégué, F. (2021). VESICAL Part I: An open-  
 909 source thermodynamic model engine for mixed volatile (H<sub>2</sub>O-CO<sub>2</sub>) solubility in silicate melts. *Earth and*  
 910 *Space Science*, 8(11), e2020EA001584. <https://doi.org/10.1029/2020EA001584>
- 911 Jackson, M. G., & Hart, S. R. (2006). Strontium isotopes in melt inclusions from Samoan basalts:  
 912 Implications for heterogeneity in the Samoan plume. *Earth and Planetary Science Letters*, 245(1–2),  
 913 260–277. <https://doi.org/10.1016/j.epsl.2006.02.040>
- 914 Jackson, M. G., & Macdonald, F. A. (2022). Hemispheric geochemical dichotomy of the mantle is a  
 915 legacy of austral supercontinent assembly and onset of deep continental crust subduction. *AGU Advances*,  
 916 3(6), e2022AV000664. <https://doi.org/10.1029/2022AV000664>
- 917 Jackson, M. G., Kurz, M. D., Hart, S. R., & Workman, R. K. (2007). New Samoan lavas from Ofu Island  
 918 reveal a hemispherically heterogeneous high <sup>3</sup>He/<sup>4</sup>He mantle. *Earth and Planetary Science*  
 919 *Letters*, 264(3–4), 360–374. <https://doi.org/10.1016/j.epsl.2007.09.023>
- 920 Jackson, M.G., Koga, K.T., Price, A., Konter, J.G., Koppers, A.A., Finlayson, V.A., Konrad, K., Hauri,  
 921 E.H., Kylander-Clark, A., Kelley, K.A., & Kendrick, M.A. (2015). Deeply dredged submarine HIMU  
 922 glasses from the Tuvalu Islands, Polynesia: Implications for volatile budgets of recycled oceanic crust.  
 923 *Geochemistry, Geophysics, Geosystems*, 16(9), 3210–3234. <https://doi.org/10.1002/2015GC005966>
- 924 Jackson, M. G., Hart, S. R., Konter, J. G., Kurz, M. D., Blusztajn, J., & Farley, K. A. (2014). Helium and  
 925 lead isotopes reveal the geochemical geometry of the Samoan plume. *Nature*, 514(7522), 355–358.  
 926 <https://doi.org/10.1038/nature13794>
- 927 Kendrick, M. A., Arculus, R., Burnard, P., & Honda, M. (2013). Quantifying brine assimilation by  
 928 submarine magmas: Examples from the Galápagos Spreading Centre and Lau Basin. *Geochimica et*  
 929 *Cosmochimica Acta*, 123, 150–165. <https://doi.org/10.1016/j.gca.2013.09.012>
- 930 Kendrick, M. A., Jackson, M. G., Kent, A. J., Hauri, E. H., Wallace, P. J., & Woodhead, J. (2014).  
 931 Contrasting behaviours of CO<sub>2</sub>, S, H<sub>2</sub>O and halogens (F, Cl, Br, and I) in enriched-mantle melts from  
 932 Pitcairn and Society seamounts. *Chemical Geology*, 370, 69–81.  
 933 <https://doi.org/10.1016/j.chemgeo.2014.01.019>
- 934 Kendrick, M. A., Hémond, C., Kamenetsky, V. S., Danyushevsky, L., Devey, C. W., Rodemann, T.,  
 935 Jackson, M. G., & Perfit, M. R. (2017). Seawater cycled throughout Earth’s mantle in partially  
 936 serpentinized lithosphere. *Nature Geoscience*, 10(3), 222–228. <https://doi.org/10.1038/ngeo2902>

- 937 Kendrick, M. A., Jackson, M. G., Hauri, E. H., & Phillips, D. (2015). The halogen (F, Cl, Br, I) and H<sub>2</sub>O  
 938 systematics of Samoan lavas: Assimilated-seawater, EM2 and high-<sup>3</sup>He/<sup>4</sup>He components. *Earth and*  
 939 *Planetary Science Letters*, 410, 197–209. <https://doi.org/10.1016/j.epsl.2014.11.026>
- 940 Kent, A. J. R., Clague, D. A., Honda, M., Stolper, E. M., Hutcheon, I. D., & Norman, M. D. (1999a).  
 941 Widespread assimilation of a seawater-derived component at Loihi Seamount, Hawaii. *Geochimica et*  
 942 *Cosmochimica Acta*, 63(18), 2749–2761. [https://doi.org/10.1016/S0016-7037\(99\)00215-X](https://doi.org/10.1016/S0016-7037(99)00215-X)
- 943 Kent, A. J. R., Norman, M. D., Hutcheon, I. D., & Stolper, E. M. (1999b). Assimilation of seawater-  
 944 derived components in an oceanic volcano: evidence from matrix glasses and glass inclusions from Loihi  
 945 seamount, Hawaii. *Chemical Geology*, 156(1–4), 299–319. [https://doi.org/10.1016/S0009-](https://doi.org/10.1016/S0009-2541(98)00188-0)  
 946 2541(98)00188-0
- 947 Kent, A. J. R., Peate, D. W., Newman, S., Stolper, E. M., & Pearce, J. A. (2002). Chlorine in submarine  
 948 glasses from the Lau Basin: seawater contamination and constraints on the composition of slab-derived  
 949 fluids. *Earth and Planetary Science Letters*, 202(2), 361–377. [https://doi.org/10.1016/S0012-](https://doi.org/10.1016/S0012-821X(02)00786-0)  
 950 821X(02)00786-0
- 951 Koleszar, A. M., Saal, A. E., Hauri, E. H., Nagle, A. N., Liang, Y., & Kurz, M. D. (2009). The volatile  
 952 contents of the Galapagos plume; evidence for H<sub>2</sub>O and F open system behavior in melt inclusions. *Earth*  
 953 *and Planetary Science Letters*, 287(3–4), 442–452. <https://doi.org/10.1016/j.epsl.2009.08.029>
- 954 Labidi, J., Cartigny, P., & Jackson, M. G. (2015). Multiple sulfur isotope composition of oxidized  
 955 Samoan melts and the implications of a sulfur isotope ‘mantle array’ in chemical geodynamics. *Earth and*  
 956 *Planetary Science Letters*, 417, 28–39. <https://doi.org/10.1016/j.epsl.2015.02.004>
- 957 Lassiter, J. C., Hauri, E. H., Nikogosian, I. K., & Barszczus, H. G. (2002). Chlorine–potassium variations  
 958 in melt inclusions from Raivavae and Rapa, Austral Islands: constraints on chlorine recycling in the  
 959 mantle and evidence for brine-induced melting of oceanic crust. *Earth and Planetary Science Letters*,  
 960 202(3–4), 525–540. [https://doi.org/10.1016/S0012-821X\(02\)00826-9](https://doi.org/10.1016/S0012-821X(02)00826-9)
- 961 Le Roux, P. J., Shirey, S. B., Hauri, E. H., Perfit, M. R., & Bender, J. F. (2006). The effects of variable  
 962 sources, processes and contaminants on the composition of northern EPR MORB (8–10°N and 12–14°N):  
 963 Evidence from volatiles (H<sub>2</sub>O, CO<sub>2</sub>, S) and halogens (F, Cl). *Earth and Planetary Science Letters*, 251(3–  
 964 4), 209–231. <https://doi.org/10.1016/j.epsl.2006.09.012>
- 965 Le Voyer, M., Kelley, K. A., Cottrell, E., & Hauri, E. H. (2017). Heterogeneity in mantle carbon content  
 966 from CO<sub>2</sub>-undersaturated basalts. *Nature Communications*, 8(1), 14062.  
 967 <https://doi.org/10.1038/ncomms14062>
- 968 Le Voyer, M., Hauri, E.H., Cottrell, E., Kelley, K.A., Salters, V.J., Langmuir, C.H., Hilton, D.R., Barry,  
 969 P.H. & Füre, E. (2019). Carbon fluxes and primary magma CO<sub>2</sub> contents along the global mid-ocean ridge  
 970 system. *Geochemistry, Geophysics, Geosystems*, 20(3), 1387–1424.  
 971 <https://doi.org/10.1029/2018GC007630>



- 972 Loewen, M. W., Graham, D. W., Bindeman, I. N., Lupton, J. E., & Garcia, M. O. (2019). Hydrogen  
 973 isotopes in high  $^3\text{He}/^4\text{He}$  submarine basalts: Primordial vs. recycled water and the veil of mantle  
 974 enrichment. *Earth and Planetary Science Letters*, 508, 62–73. <https://doi.org/10.1016/j.epsl.2018.12.012>
- 975 Machida, S., Hirano, N., Sumino, H., Hirata, T., Yoneda, S. & Kato, Y. (2015). Petit-spot geology reveals  
 976 melts in upper-most asthenosphere dragged by lithosphere. *Earth and Planetary Science Letters*, 426,  
 977 267–279. <https://doi.org/10.1016/j.epsl.2015.06.018>
- 978 Matthews, S., Shorttle, O., Maclennan, J., & Rudge, J. F. (2021). The global melt inclusion C/Ba array:  
 979 Mantle variability, melting process, or degassing?. *Geochimica et Cosmochimica Acta*, 293, 525–543.  
 980 <https://doi.org/10.1016/j.gca.2020.09.030>
- 981 McDonough, W. F., & Sun, S. S. (1995). The composition of the Earth. *Chemical Geology*, 120, 223–  
 982 253. [https://doi.org/10.1016/0009-2541\(94\)00140-4](https://doi.org/10.1016/0009-2541(94)00140-4)
- 983 Métrich, N., Zanon, V., Créon, L., Hildenbrand, A., Moreira, M., & Marques, F. O. (2014). Is the ‘Azores  
 984 hotspot’ a wet spot? Insights from the geochemistry of fluid and melt inclusions in olivine of Pico basalts.  
 985 *Journal of Petrology*, 55(2), 377–393. <https://doi.org/10.1093/petrology/egt071>
- 986 Miller, W. G., Maclennan, J., Shorttle, O., Gaetani, G. A., Le Roux, V., & Klein, F. (2019). Estimating  
 987 the carbon content of the deep mantle with Icelandic melt inclusions. *Earth and Planetary Science  
 988 Letters*, 523, 115699. <https://doi.org/10.1016/j.epsl.2019.07.002>
- 989 Michael, P. (1995). Regionally distinctive sources of depleted MORB: Evidence from trace elements and  
 990  $\text{H}_2\text{O}$ . *Earth and Planetary Science Letters*, 131(3-4), 301–320. [https://doi.org/10.1016/0012-  
 991 821X\(95\)00023-6](https://doi.org/10.1016/0012-821X(95)00023-6)
- 992 Michael, P. J., & Graham, D. W. (2015). The behavior and concentration of  $\text{CO}_2$  in the suboceanic  
 993 mantle: Inferences from undegassed ocean ridge and ocean island basalts. *Lithos*, 236, 338–351.  
 994 <https://doi.org/10.1016/j.lithos.2015.08.020>
- 995 Moore, L.R., Gazel, E., Tuohy, R., Lloyd, A.S., Esposito, R., Steele-MacInnis, M., Hauri, E.H., Wallace,  
 996 P.J., Plank, T. & Bodnar, R.J. (2015). Bubbles matter: An assessment of the contribution of vapor bubbles  
 997 to melt inclusion volatile budgets. *American Mineralogist*, 100(4), 806–823. [https://doi.org/10.2138/am-  
 998 2015-5036](https://doi.org/10.2138/am-2015-5036)
- 999 Portnyagin, M., Almeev, R., Matveev, S., & Holtz, F. (2008). Experimental evidence for rapid water  
 1000 exchange between melt inclusions in olivine and host magma. *Earth and Planetary Science Letters*,  
 1001 272(3–4), 541–552. <https://doi.org/10.1016/j.epsl.2008.05.020>
- 1002 Portnyagin, M., Hoernle, K., Plechov, P., Mironov, N., & Khubunaya, S. (2007). Constraints on mantle  
 1003 melting and composition and nature of slab components in volcanic arcs from volatiles ( $\text{H}_2\text{O}$ , S, Cl, F)  
 1004 and trace elements in melt inclusions from the Kamchatka Arc. *Earth and Planetary Science  
 1005 Letters*, 255(1-2), 53–69. <https://doi.org/10.1016/j.epsl.2006.12.005>
- 1006 Reinhard, A.A., Jackson, M.G., Koornneef, J.M., Rose-Koga, E.F., Blusztajn, J., Konter, J.G., Koga,  
 1007 K.T., Wallace, P.J. & Harvey, J. (2018). Sr and Nd isotopic compositions of individual olivine-hosted  
 1008 melt inclusions from Hawai'i and Samoa: Implications for the origin of isotopic heterogeneity in melt

- 1009 inclusions from OIB lavas. *Chemical Geology*, 495, 36–49.  
 1010 <https://doi.org/10.1016/j.chemgeo.2018.07.034>
- 1011 Roeder, P.L., & Emslie, R. (1970). Olivine-liquid equilibrium. *Contributions to Mineralogy and*  
 1012 *Petrology*, 29(4), 275–289. <https://doi.org/10.1007/BF00371276>
- 1013 Rose-Koga, E.F., Koga, K.T., Moreira, M., Vlastélic, I., Jackson, M.G., Whitehouse, M.J., Shimizu, N.,  
 1014 & Habib, N. (2017). Geochemical systematics of Pb isotopes, fluorine, and sulfur in melt inclusions from  
 1015 São Miguel, Azores. *Chemical Geology*, 458, 22–37. <https://doi.org/10.1016/j.chemgeo.2017.03.024>
- 1016 Rose-Koga, E.F., Koga, K.T., Schiano, P., Le Voyer, M., Shimizu, N., Whitehouse, M.J., Clocchiatti, R.,  
 1017 2012. Mantle source heterogeneity for South Tyrrhenian magmas revealed by Pb isotopes and halogen  
 1018 contents of olivine-hosted melt inclusions. *Chemical Geology*, 334, 266–279.  
 1019 <https://doi.org/10.1016/j.chemgeo.2012.10.033>
- 1020 Rowe, M. C., & Lassiter, J. C. (2009). Chlorine enrichment in central Rio Grande Rift basaltic melt  
 1021 inclusions: Evidence for subduction modification of the lithospheric mantle. *Geology*, 37(5), 439–442.  
 1022 <https://doi.org/10.1130/G25530A.1>
- 1023 Ryan, W. B. F., Carbotte, S. M., Coplan, J. O., O'Hara, S., Melkonian, A., Arko, R., Weissel, R. A.,  
 1024 Ferrini, V., Goodwillie, A., Nitsche, F., Bonczkowski, J., & Zemsky, R. (2009). Global Multi-Resolution  
 1025 Topography synthesis. *Geochemistry, Geophysics, Geosystems*, 10, Q03014.  
 1026 <https://doi.org/10.1029/2008GC002332>
- 1027 Saal, A. E., Hauri, E. H., Langmuir, C. H., & Perfit, M. R. (2002). Vapour undersaturation in primitive  
 1028 mid-ocean-ridge basalt and the volatile content of Earth's upper mantle. *Nature*, 419(6906), 451–455.  
 1029 <https://doi.org/10.1038/nature01073>
- 1030 Shimizu, K., Saal, A. E., Hauri, E. H., Sinton, J. M., Janney, P. E., Geshi, N., & Hékinian, R. (2023).  
 1031 High-C content and CO<sub>2</sub>/Ba ratio of the Earth's enriched upper mantle. *Geochimica et Cosmochimica*  
 1032 *Acta*. <https://doi.org/10.1016/j.gca.2022.10.023>
- 1033 Shimizu, K., Saal, A.E., Myers, C.E., Nagle, A.N., Hauri, E.H., Forsyth, D.W., Kamenetsky, V.S., & Niu,  
 1034 Y. (2016). Two-component mantle melting-mixing model for the generation of mid-ocean ridge basalts:  
 1035 Implications for the volatile content of the Pacific upper mantle. *Geochimica et Cosmochimica Acta*, 176,  
 1036 44–80. <https://doi.org/10.1016/j.gca.2015.10.033>
- 1037 Sims, K. W. W., Hart, S.R., Reagan, M.K., Blusztajn, J., Staudigel, H., Sohn, R.A., Layne, G.D., Ball,  
 1038 L.A., & Andrews, J. (2008). 238U-230Th-226Ra-210Pb-210Po, 232Th-228Ra, and 235U-231Pa  
 1039 constraints on the ages and petrogenesis of Vailulu'u and Malumalu Lavas, Samoa. *Geochemistry,*  
 1040 *Geophysics, Geosystems*, 9, Q04003. <https://doi.org/10.1029/2007GC001651>.
- 1041 Smythe, D. J., Wood, B. J., & Kiseeva, E. S. (2017). The S content of silicate melts at sulfide saturation:  
 1042 new experiments and a model incorporating the effects of sulfide composition. *American Mineralogist*,  
 1043 102(4), 795–803. <https://doi.org/10.2138/am-2017-5800CCBY>

- 1044 Staudigel, H., Zindler, A., Hart, S. R., Leslie, T., Chen, C. Y., & Clague, D. (1984). The isotope  
 1045 systematics of a juvenile intraplate volcano: Pb, Nd, and Sr isotope ratios of basalts from Loihi Seamount,  
 1046 Hawaii. *Earth and Planetary Science Letters*, 69(1), 13–29. [https://doi.org/10.1016/0012-](https://doi.org/10.1016/0012-821X(84)90071-2)  
 1047 821X(84)90071-2
- 1048 Sun, C., & Dasgupta, R. (2020). Thermobarometry of CO<sub>2</sub>-rich, silica-undersaturated melts constrains  
 1049 cratonic lithosphere thinning through time in areas of kimberlitic magmatism. *Earth and Planetary*  
 1050 *Science Letters*, 550, 116549. <https://doi.org/10.1016/j.epsl.2020.116549>
- 1051 Taracsák, Z., Hartley, M. E., Burgess, R., Edmonds, M., Iddon, F., & Longpré, M. A. (2019). High fluxes  
 1052 of deep volatiles from ocean island volcanoes: Insights from El Hierro, Canary Islands. *Geochimica et*  
 1053 *Cosmochimica Acta*, 258, 19–36. <https://doi.org/10.1016/j.gca.2019.05.020>
- 1054 Wallace, P. J. (2002). Volatiles in submarine basaltic glasses from the Northern Kerguelen Plateau (ODP  
 1055 Site 1140): Implications for source region compositions, magmatic processes, and plateau subsidence.  
 1056 *Journal of Petrology*, 43(7), 1311–1326. <https://doi.org/10.1093/petrology/43.7.1311>
- 1057 Wanless, V. D., & Shaw, A. M. (2012). Lower crustal crystallization and melt evolution at mid-ocean  
 1058 ridges. *Nature Geoscience*, 5(9), 651–655. <https://doi.org/10.1038/ngeo1552>
- 1059 Wanless, V. D., Behn, M. D., Shaw, A. M., & Plank, T. (2014). Variations in melting dynamics and  
 1060 mantle compositions along the Eastern Volcanic Zone of the Gakkel Ridge: insights from olivine-hosted  
 1061 melt inclusions. *Contributions to Mineralogy and Petrology*, 167, 1–22. [https://doi.org/10.1007/s00410-](https://doi.org/10.1007/s00410-014-1005-7)  
 1062 014-1005-7
- 1063 Wanless, V. D., Shaw, A. M., Behn, M. D., Soule, S. A., Escartín, J., & Hamelin, C. (2015). Magmatic  
 1064 plumbing at Lucky Strike volcano based on olivine-hosted melt inclusion compositions. *Geochemistry,*  
 1065 *Geophysics, Geosystems*, 16(1), 126–147. <https://doi.org/10.1002/2014GC005517>
- 1066 White, W. M., & Duncan, R. A. (1996). Geochemistry and geochronology of the Society Islands: New  
 1067 evidence for deep mantle recycling. *Geophysical Monograph-American Geophysical Union*, 95, 183–206.
- 1068 White, W. M., & Hofmann, A. W. (1982). Sr and Nd isotope geochemistry of oceanic basalts and mantle  
 1069 evolution. *Nature*, 296(5860), 821–825. <https://doi.org/10.1038/296821a0>
- 1070 Wieser, P. E., Iacovino, K., Matthews, S., Moore, G., & Allison, C. M. (2022). VESICAL: 2. A Critical  
 1071 Approach to Volatile Solubility Modeling Using an Open-Source Python3 Engine. *Earth and Space*  
 1072 *Science*, 9(2), e2021EA001932. <https://doi.org/10.1029/2021EA001932>
- 1073 Workman, R.K., Hart, S.R., Jackson, M., Regelous, M., Farley, K.A., Blusztajn, J., Kurz, M. & Staudigel,  
 1074 H. (2004). Recycled metasomatized lithosphere as the origin of the Enriched Mantle II (EM2) end-  
 1075 member: Evidence from the Samoan Volcanic Chain. *Geochemistry, Geophysics, Geosystems*, 5(4).  
 1076 <https://doi.org/10.1029/2003GC000623>
- 1077 Workman, R. K., Hauri, E., Hart, S. R., Wang, J., & Blusztajn, J. (2006). Volatile and trace elements in  
 1078 basaltic glasses from Samoa: Implications for water distribution in the mantle. *Earth and Planetary*  
 1079 *Science Letters*, 241(3–4), 932–951. <https://doi.org/10.1016/j.epsl.2005.10.028>

1080 Woodhead, J. D., & Devey, C. W. (1993). Geochemistry of the Pitcairn seamounts, I: source character  
1081 and temporal trends. *Earth and Planetary Science Letters*, 116(1–4), 81–99. [https://doi.org/10.1016/0012-](https://doi.org/10.1016/0012-821X(93)90046-C)  
1082 821X(93)90046-C

1083

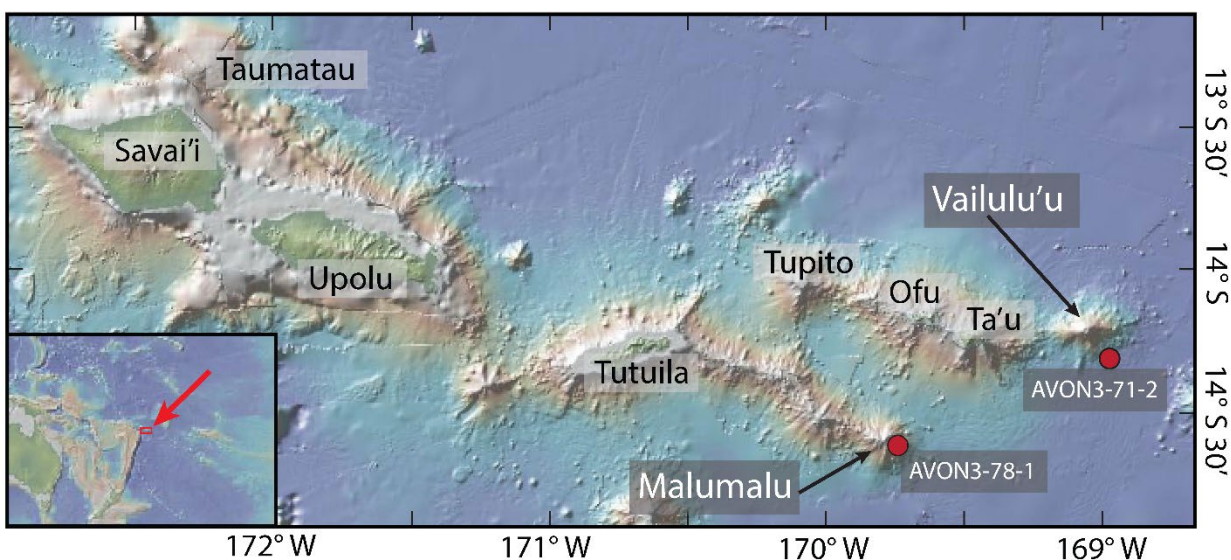
1084

1085

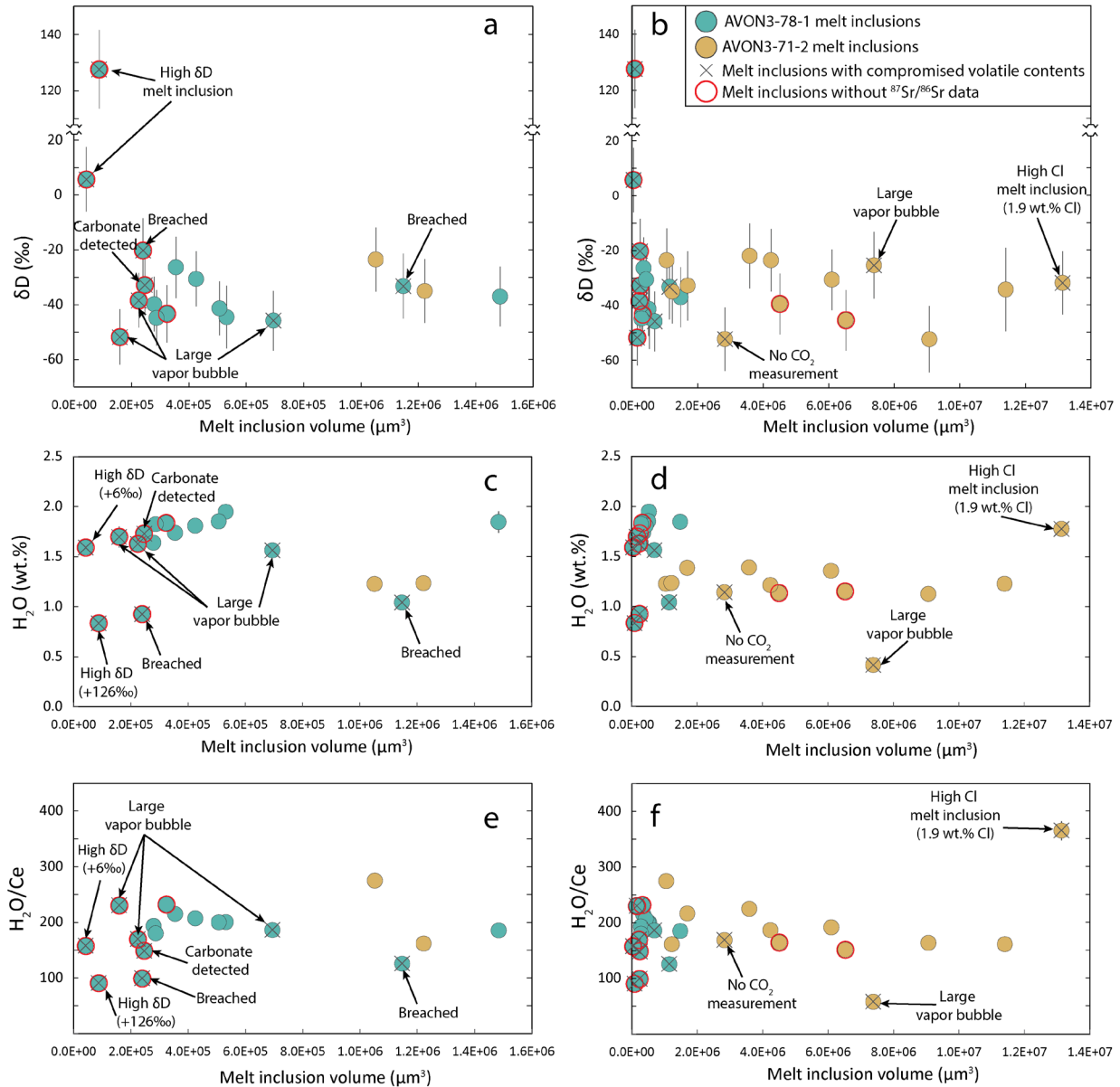
1086

1087

1088 **FIGURES**



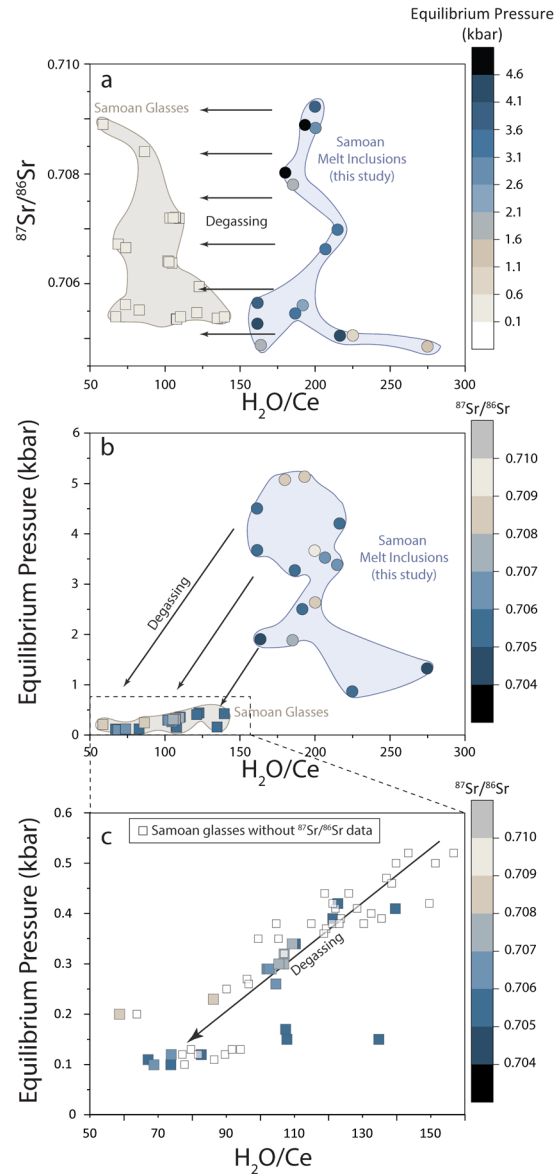
1089 **Figure 1.** Map of the Samoan Islands. Red dots indicate the location of AVON3 cruise dredge sites 71 and  
1090 78, from the flanks of Vailulu'u and Malumalu, respectively. Map created using GeoMapApp  
1091 ([www.geomapapp.org](http://www.geomapapp.org)).



1092

1093 **Figure 2. (a–b)  $\delta D$  (‰), (c–d)  $H_2O$  (wt.%), and (e–f)  $H_2O/Ce$  versus melt inclusion volume ( $\mu m^3$ ).** Left-  
 1094 hand side panels focus (zoom in) on the Malumalu melt inclusions and right-hand side panels (zoom out)  
 1095 to show the Vailulu'u melt inclusions. In panel (a)  $\delta D$  errors represent the  $2\sigma$  in run measurement  
 1096 precision of each analysis, which is generally slightly lower than the reproducibility of the secondary  
 1097 standard ALV1833-1 (i.e.,  $\pm 16\%$ , 2SD; see Table S2). Melt inclusion  $H_2O$  compositions are corrected for  
 1098 olivine addition/subtraction to be in equilibrium with the host olivine (olivine correction is as in Section  
 1099 2 of the main text). Measurement errors for  $H_2O$ , and reproducibility of  $H_2O$  analyses on ALV1833-1, are  
 1100 smaller than the data symbol (see Table S2). As discussed in Section 3 of the text, we infer that the  
 1101 volatile contents of eleven melt inclusions shown in this figure have been compromised in one of several  
 1102 ways—hydrogen diffusion loss (and resultant elevated  $\delta D$ ), breaching, large vapor bubbles, extremely  
 1103 high Cl concentrations, presence of carbonate, and/or missing Raman-based  $CO_2$  data—and are marked  
 1104 with an “x” symbol. With the exception of the high Cl melt inclusion (which is individually identified in

1105 figures throughout the paper), the compromised melt inclusions are not shown in subsequent volatile  
 1106 element figures.

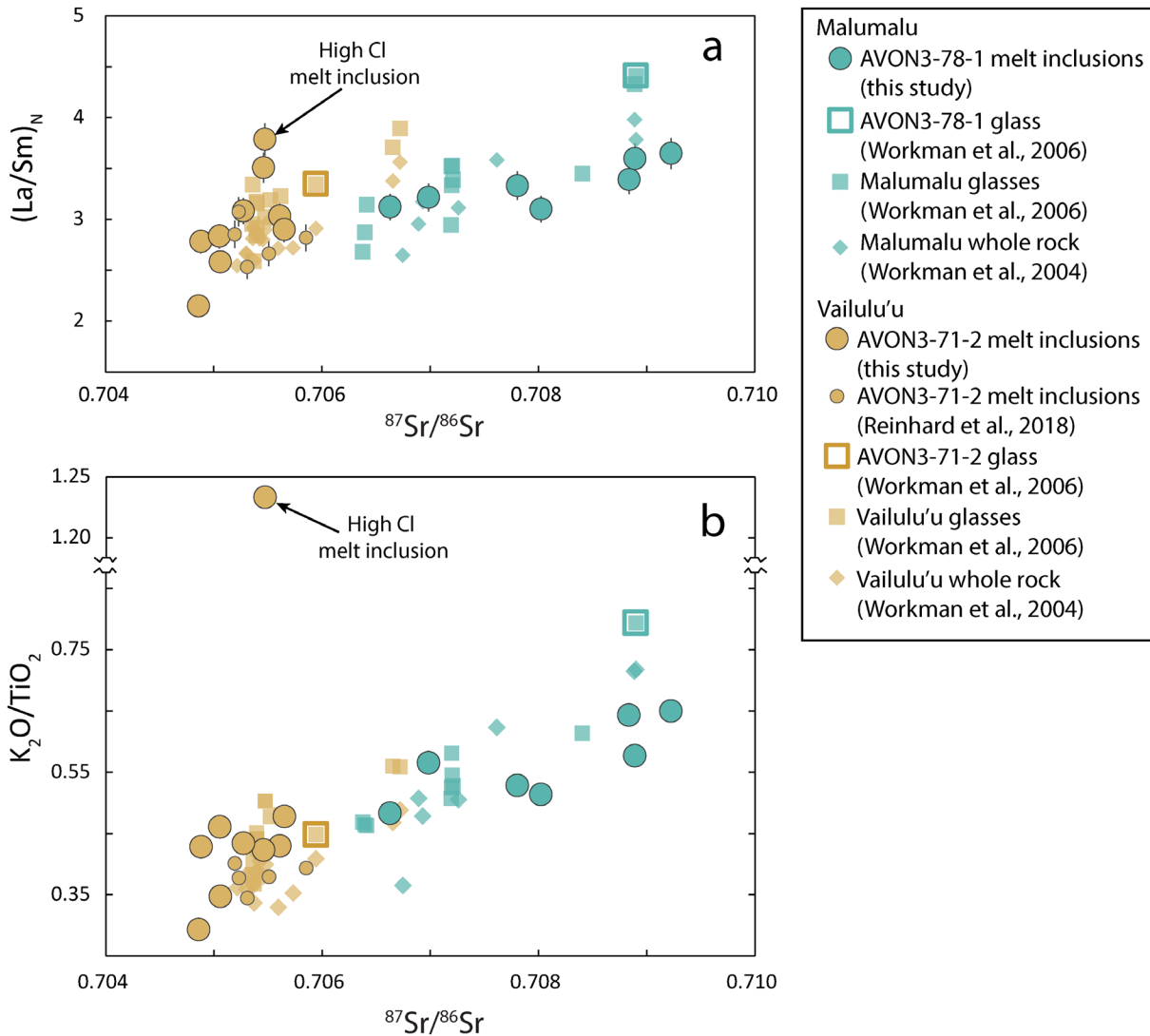


1107

1108 **Figure 3.**  $^{87}\text{Sr}/^{86}\text{Sr}$ ,  $\text{H}_2\text{O}/\text{Ce}$ , and equilibrium pressure for submarine pillow glasses from Malumalu and  
 1109 Vailulu'u seamounts are compared with melt inclusions from Malumalu sample AVON3-78-1 and  
 1110 Vailulu'u sample AVON3-71-2. (a)  $^{87}\text{Sr}/^{86}\text{Sr}$  versus  $\text{H}_2\text{O}/\text{Ce}$  for Samoan melt inclusions and glasses with  
 1111 the color bar representing equilibrium pressure (kbar). The pillow glass data show separation in  $\text{H}_2\text{O}/\text{Ce}$   
 1112 from the melt inclusion data, even though both datasets span a similar range in  $^{87}\text{Sr}/^{86}\text{Sr}$ . Circles  
 1113 represent melt inclusions and squares represent Samoan pillow glasses from Workman et al. (2006).  
 1114 Melt inclusions in this figure do not include any volatile-compromised melt inclusions (as shown in  
 1115 Figure 2). The equilibrium pressure of pillow glasses and melt inclusions was calculated using VESIcal's  
 1116 MagmaSat model (Iacovino et al., 2021; Wieser et al., 2022) assuming oxygen fugacity (QFM) and  
 1117 temperature (1200°C). Samoan pillow glass data are from Workman et al. (2006), except major elements  
 1118 used to calculate equilibrium pressure for AVON3-71-2 and AVON3-78-1 (which are from Kendrick et al.,

1119 2015). (b) Equilibrium pressure versus H<sub>2</sub>O/Ce for Samoan melt inclusions and pillow glasses with the  
 1120 color bar representing <sup>87</sup>Sr/<sup>86</sup>Sr. (c) Expanded view of panel b that shows equilibrium pressure versus  
 1121 H<sub>2</sub>O/Ce for Samoan pillow glasses only. Smaller square data points with black outlines are pillow glasses  
 1122 lacking <sup>87</sup>Sr/<sup>86</sup>Sr data. Only samples with CO<sub>2</sub>-H<sub>2</sub>O saturation pressures ≥0.1 kbar are shown (just one  
 1123 Samoan glass with <sup>87</sup>Sr/<sup>86</sup>Sr data has a saturation pressure <0.1 kbar, sample AVON3-68-03 Rpt, so its  
 1124 removal does not significantly impact the dataset).

1125

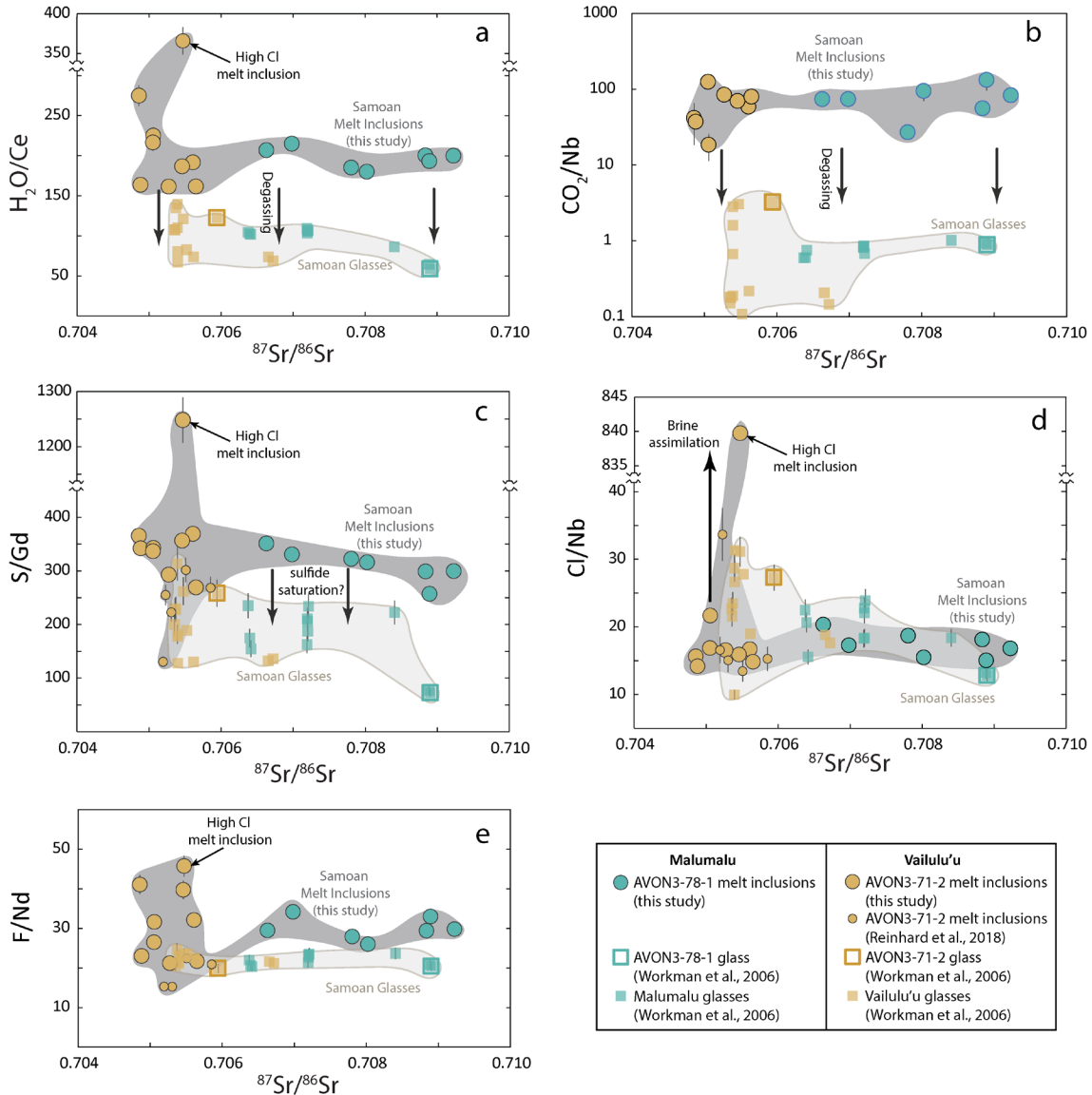


1126

1127 **Figure 4.** Incompatible trace element ratios versus <sup>87</sup>Sr/<sup>86</sup>Sr are shown for Samoan pillow glasses from  
 1128 Malumalu and Vailulu'u seamounts and new melt inclusion data from Malumalu sample AVON3-78-1  
 1129 and Vailulu'u sample AVON3-71-2. The melt inclusions have incompatible trace element ratios and  
 1130 <sup>87</sup>Sr/<sup>86</sup>Sr compositions that fall within the range identified in Samoan pillow glasses, indicating that the  
 1131 Samoan melt inclusions sample melts represented by the pillow glass dataset. (a) (La/Sm)<sub>N</sub> versus  
 1132 <sup>87</sup>Sr/<sup>86</sup>Sr, where N signifies normalization to primitive mantle (McDonough & Sun, 1995). (b) K<sub>2</sub>O/TiO<sub>2</sub>



1133 versus  $^{87}\text{Sr}/^{86}\text{Sr}$ . Data for Samoan pillow glasses are from Workman et al. (2006) and Kendrick et al.  
 1134 (2015). Error bars for La/Sm (4.2%) are shown for the melt inclusions and are calculated as  $((\text{La error})^2 + (\text{Sm error})^2)^{0.5}$ , where the 2RSD of the secondary standard BCR-2 is used for La error (1.9%) and  
 1135 Sm error (3.8%) (see Table S2). Error bars on  $\text{K}_2\text{O}/\text{TiO}_2$  are smaller than the data symbols. Melt inclusions  
 1137 that are compromised with respect to their volatile contents are not shown, except for the high Cl melt  
 1138 inclusion.



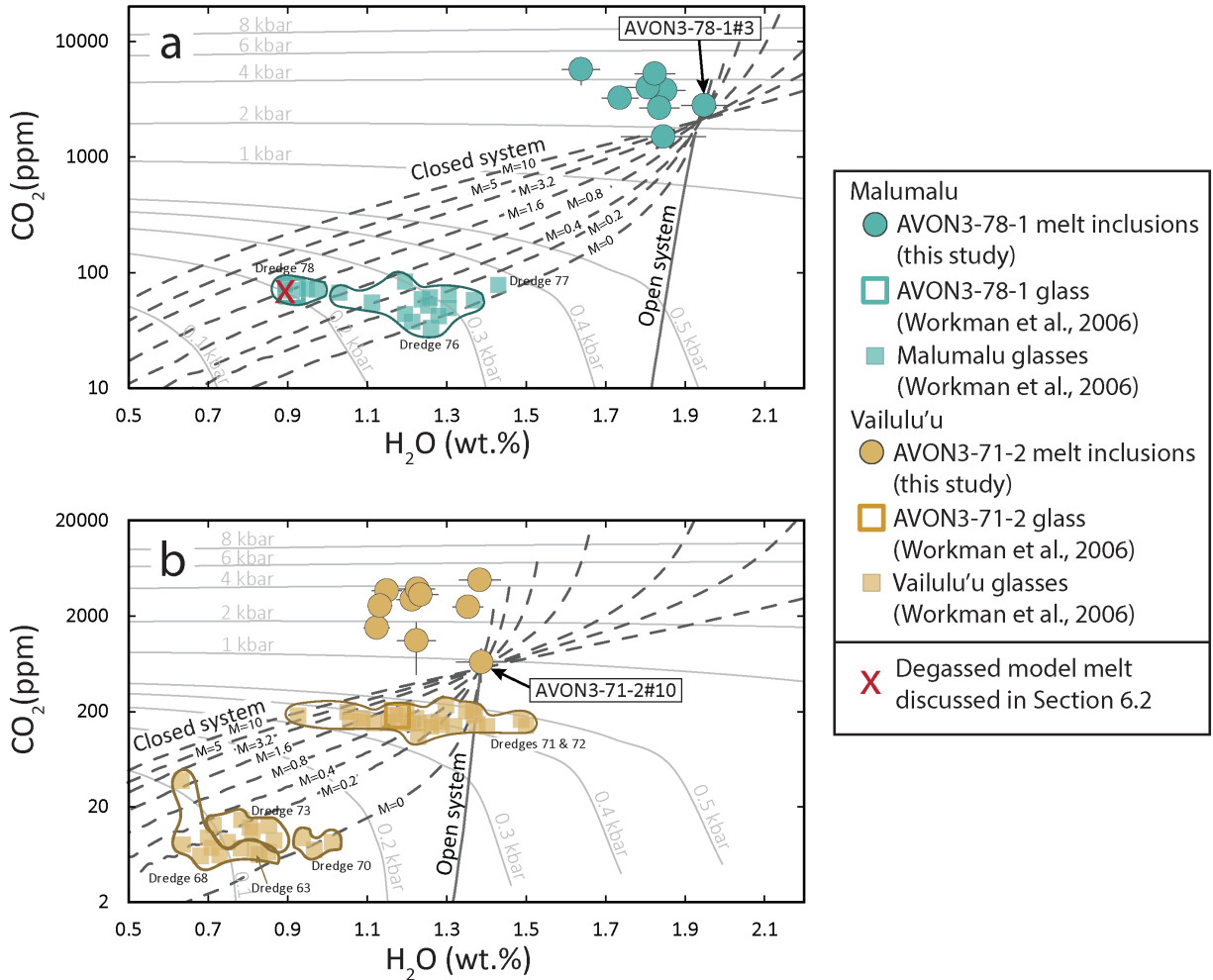
1139  
 1140 **Figure 5.** Element ratios (volatile/incompatible trace element) are plotted against  $^{87}\text{Sr}/^{86}\text{Sr}$  for Samoan  
 1141 pillow glasses from Malumalu and Vailulu'u seamounts and the new melt inclusion data from Malumalu  
 1142 sample AVON3-78-1 and Vailulu'u sample AVON3-71-2. See Supplementary Text section S1.6 for a  
 1143 discussion on the calculation of the errors associated with the element ratios presented here; the error  
 1144 bars for the  $^{87}\text{Sr}/^{86}\text{Sr}$  of Samoan glasses and melt inclusions are smaller than the symbol size. Melt  
 1145 inclusions that are compromised with respect to their volatile contents (as shown in Figure 2) are not



1146 shown. Only samples with CO<sub>2</sub>-H<sub>2</sub>O saturation pressures ≥0.1 kbar are shown (just one Samoan glass  
 1147 with <sup>87</sup>Sr/<sup>86</sup>Sr data has a saturation pressure <0.1 kbar, sample AVON3-68-03 Rpt, so its removal does  
 1148 not significantly impact the dataset).

1149

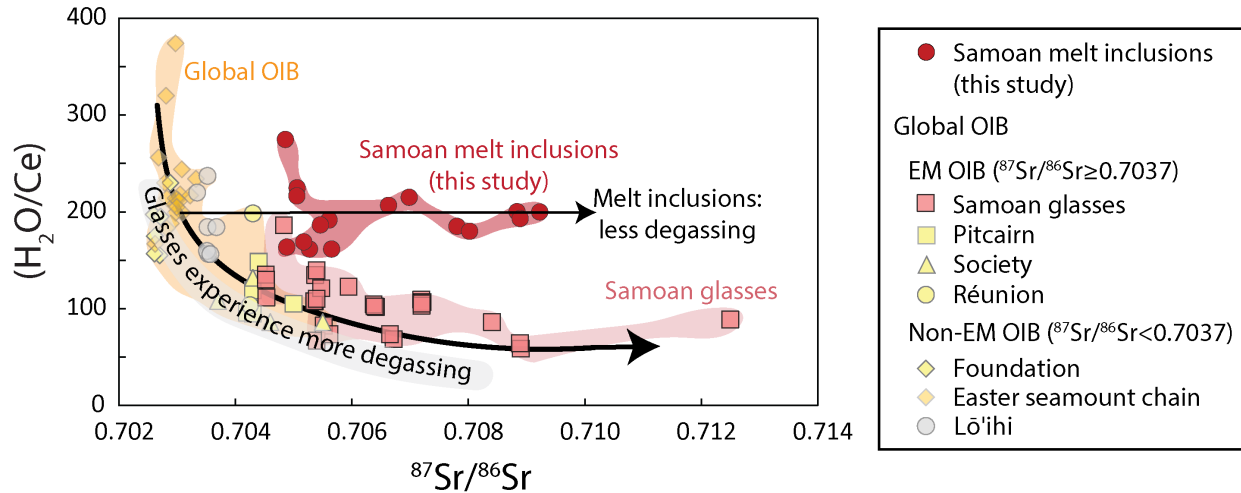
1150



1151

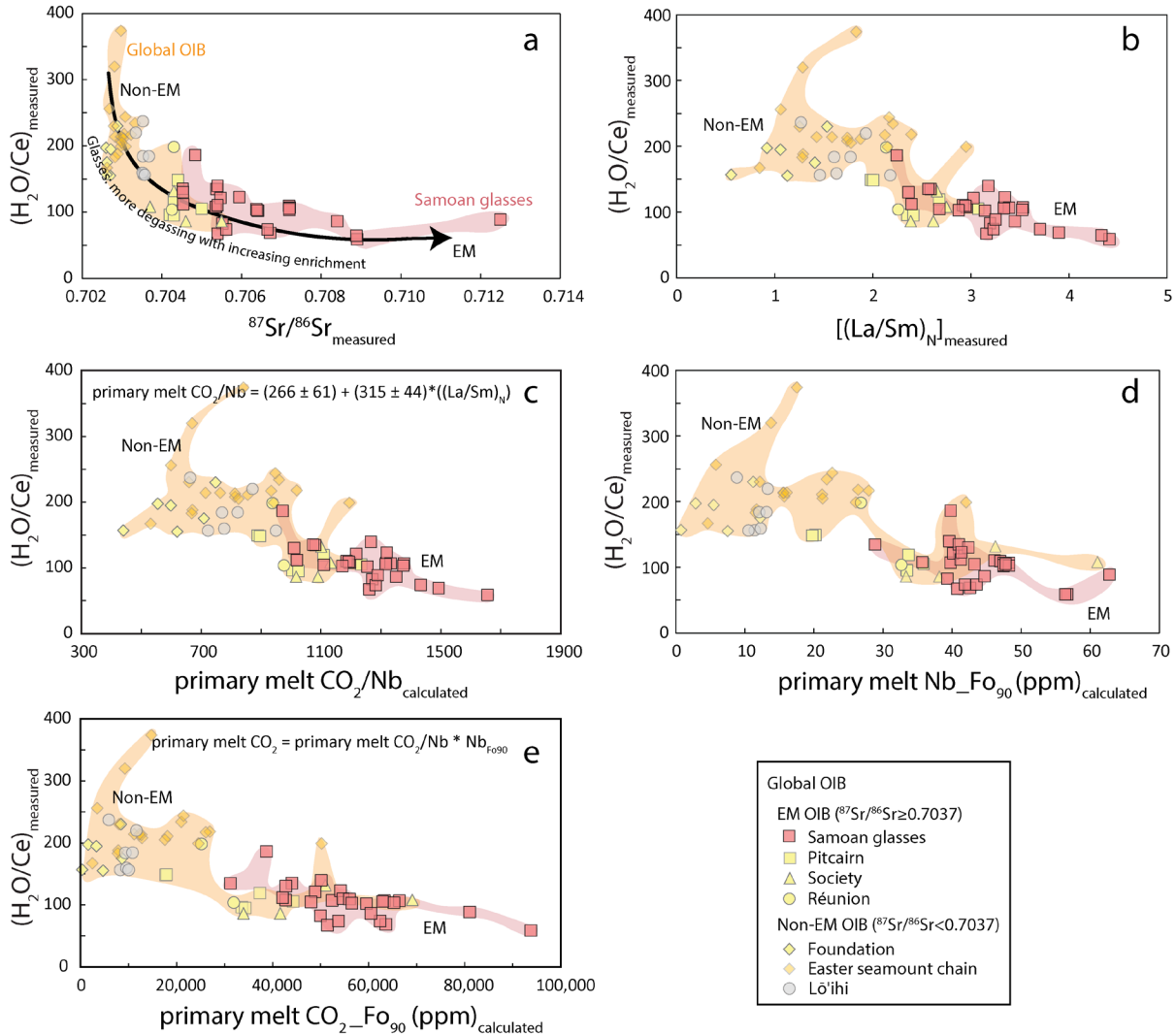
1152 **Figure 6.** CO<sub>2</sub> versus H<sub>2</sub>O for (a) melt inclusions from Malumalu sample AVON3-78-1 and all glasses from  
 1153 Malumalu seamount and (b) melt inclusions from Vailulu'u sample AVON3-71-2 and all glasses from  
 1154 Vailulu'u seamount. Melt inclusion data are from this study and Samoan glass data are from Workman  
 1155 et al. (2006) and the data are shown in fields separated by the dredge number (which is provided next to  
 1156 the relevant field). Isobars are calculated using MagmaSat for an average melt inclusion composition of  
 1157 each sample at 1200°C. Closed system degassing curves are calculated with varying values for M (where  
 1158 “M” represents mass fraction of equilibrium fluid in the magma; e.g., M=1.6 means there was 1.6 wt.%  
 1159 of fluid in the magma before degassing). Degassing trends assume an oxygen fugacity (QFM) and  
 1160 temperature (1200°C) and are calculated in rhyolite-MELTS v1.2 using H<sub>2</sub>O and CO<sub>2</sub> compositions that  
 1161 match the highest H<sub>2</sub>O melt inclusions in the respective panels (i.e., Malumalu melt inclusion AVON3-78-

1162 1#3 in the upper panel, and Vailulu'u melt inclusion AVON3-71-2#10 in the lower panel); other  
 1163 compositions used in the degassing calculation are in Table S9. Melt inclusion CO<sub>2</sub> and H<sub>2</sub>O  
 1164 concentrations shown are values that have been corrected to be in equilibrium with the host olivine.  
 1165 Volatile-compromised melt inclusions (as shown in Figure 2) are not included in this figure.



1166

1167 **Figure 7.** Samoan melt inclusions and pillow glasses compared to a global dataset of submarine OIB  
 1168 glasses. Samoan melt inclusions—protected from the extensive degassing experienced by Samoan  
 1169 glasses—have higher H<sub>2</sub>O/Ce than Samoan pillow glasses, and thus fall off of the global submarine OIB  
 1170 pillow glass trend that shows decreasing H<sub>2</sub>O/Ce with increasing <sup>87</sup>Sr/<sup>86</sup>Sr. Only OIB glasses with <sup>87</sup>Sr/<sup>86</sup>Sr  
 1171 (to establish the level of source enrichment) and MgO > 4.5 wt.% (to minimize the impact of fractional  
 1172 crystallization) are shown. Sources of data (see Table S11): Pitcairn (Kendrick et al., 2014; Woodhead &  
 1173 Devey, 1993), Society (Devey et al., 1990; Kendrick et al., 2014), Réunion (Kendrick et al., 2017; Fretzdorf  
 1174 & Haase, 2002), Foundation (Kendrick et al., 2017), Easter seamount chain (Dixon et al., 2002), Lō'ihi  
 1175 (Dixon & Clague, 2001; Staudigel et al., 1984). Samples from Pitcairn, Society, Réunion, and Foundation  
 1176 can be found in a data compilation by Kendrick et al. (2017). Samples marked as having experienced  
 1177 assimilation of seawater Cl in Kendrick et al. (2017) are excluded. However, unlike Dixon et al. (2002),  
 1178 we do not use H<sub>2</sub>O/Ce as a filter for assimilation. Samoan pillow glasses include submarine glasses  
 1179 characterized for <sup>87</sup>Sr/<sup>86</sup>Sr from Vailulu'u, Malumalu, Tupito (formerly known as Muli), Taumatau, and  
 1180 Ta'u (Kendrick et al., 2015; Workman et al., 2006). Volatile-compromised melt inclusions (as shown in  
 1181 Figure 2) are not shown. Melt inclusions from other OIB localities are not shown because there are no  
 1182 other OIB melt inclusions characterized for both <sup>87</sup>Sr/<sup>86</sup>Sr and H<sub>2</sub>O/Ce. Only samples with CO<sub>2</sub>-H<sub>2</sub>O  
 1183 saturation pressures ≥ 0.1 kbar are shown (just one Samoan glass with <sup>87</sup>Sr/<sup>86</sup>Sr data has a saturation  
 1184 pressure < 0.1 kbar, sample AVON3-68-03 Rpt, so its removal does not significantly impact the dataset).

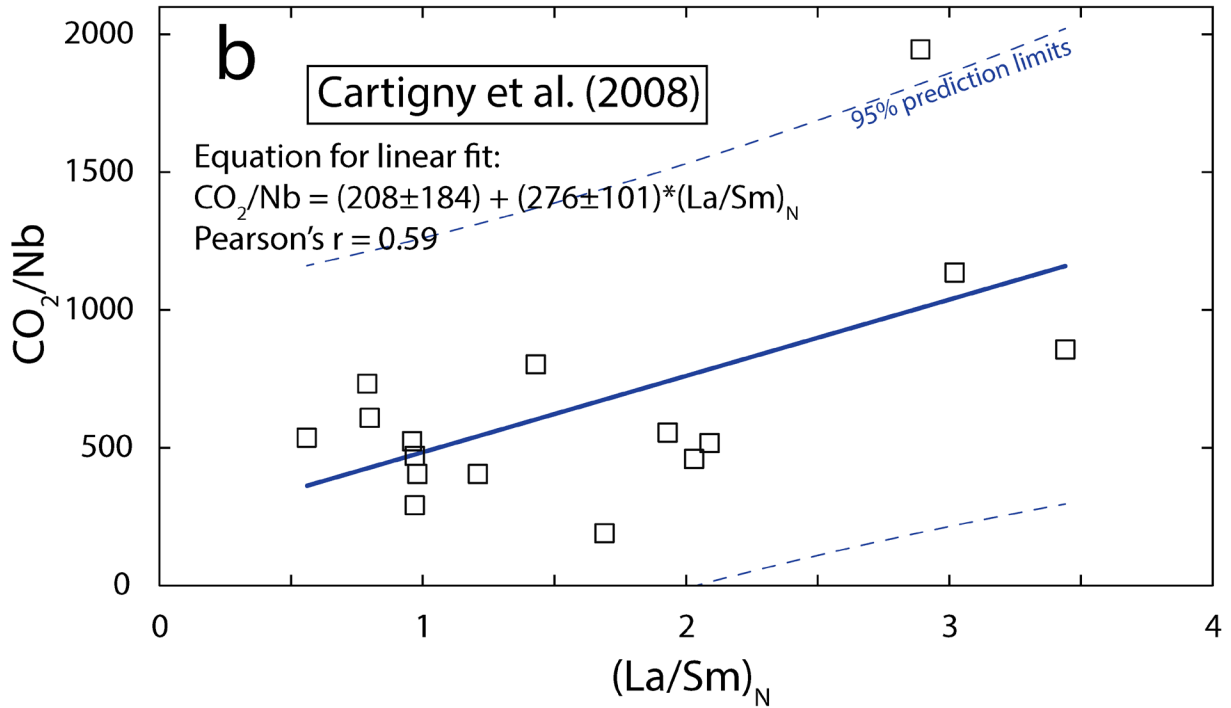
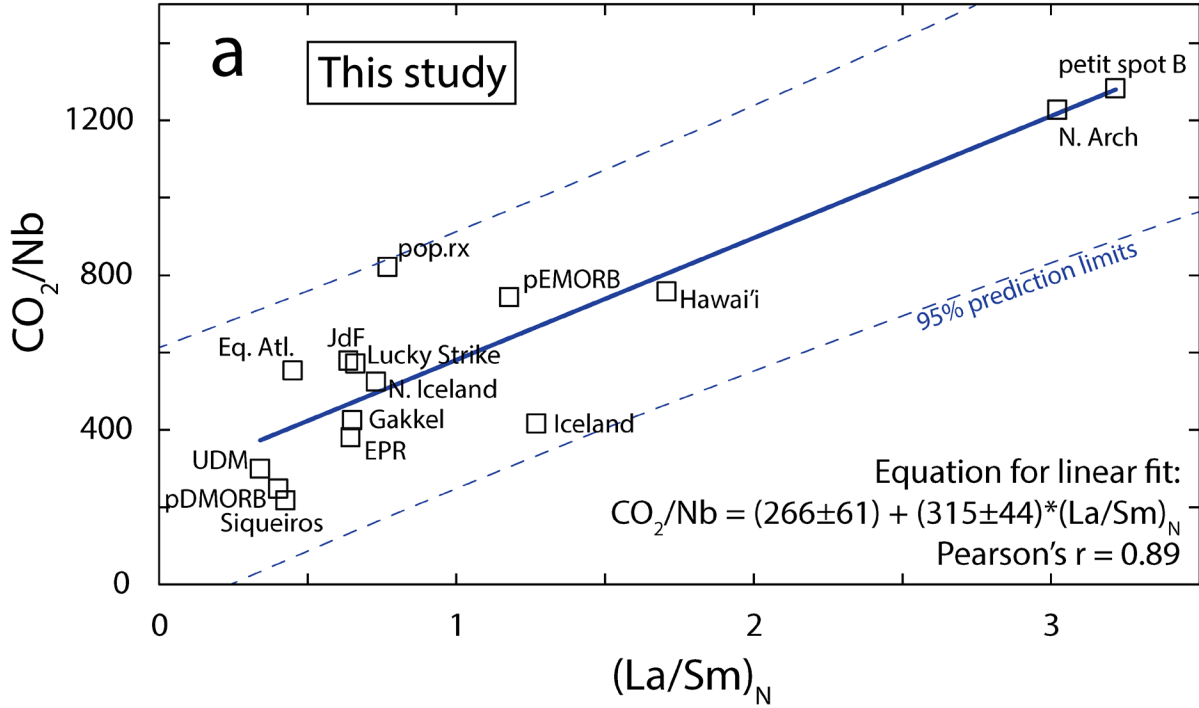


1185

1186 **Figure 8.** Samoan pillow glasses compared to a global dataset of submarine OIB glasses, which show a  
 1187 trend of decreasing  $H_2O/Ce$  with increasing  $^{87}Sr/^{86}Sr$ . The exact same OIB dataset is shown in all panels:  
 1188 only OIB with  $^{87}Sr/^{86}Sr$  data (to establish the level of source enrichment) and  $MgO > 4.5$  wt.% (to  
 1189 minimize the impact of fractional crystallization) are shown. (a)  $H_2O/Ce$  versus  $^{87}Sr/^{86}Sr$ . (b)  $H_2O/Ce$   
 1190 versus  $(La/Sm)_N$ . (c)  $H_2O/Ce$  versus primary melt  $CO_2/Nb$ , where  $CO_2/Nb$  is calculated from the measured  
 1191  $(La/Sm)_N$  ratios using a linear fit between  $CO_2/Nb$  and  $(La/Sm)_N$  (see equation shown in panel c) that is  
 1192 produced from a global data compilation of least degassed glasses and melt inclusions from OIB and  
 1193 MORB in Figure 9. (d)  $H_2O/Ce$  versus calculated primary melt Nb for each sample, where primary melt  
 1194 Nb is calculated by olivine addition (or subtraction) from melt—following methods in text—until the  
 1195 melt is in equilibrium with  $Fo_{90}$  olivine. (e)  $H_2O/Ce$  versus calculated primary melt  $CO_2$ , where the  $CO_2$   
 1196 is calculated for each lava by multiplying the calculated  $CO_2/Nb$  (panel c) with the calculated primary melt  
 1197 Nb (panel d) (see equation in panel e). The same sources of data and data treatment as that described in  
 1198 the Figure 7 caption are used here. The calculated primary melt  $CO_2/Nb$  and  $CO_2_{Fo_{90}}$  (ppm) values for  
 1199 the global OIB data set presented here are given in Table S11. Only samples with  $CO_2$ - $H_2O$  saturation

1200 pressures  $\geq 0.1$  kbar are shown (just one Samoan glass with  $^{87}\text{Sr}/^{86}\text{Sr}$  data has a saturation pressure  $< 0.1$   
 1201 kbar, sample AVON3-68-03 Rpt, so its removal does not significantly impact the dataset).

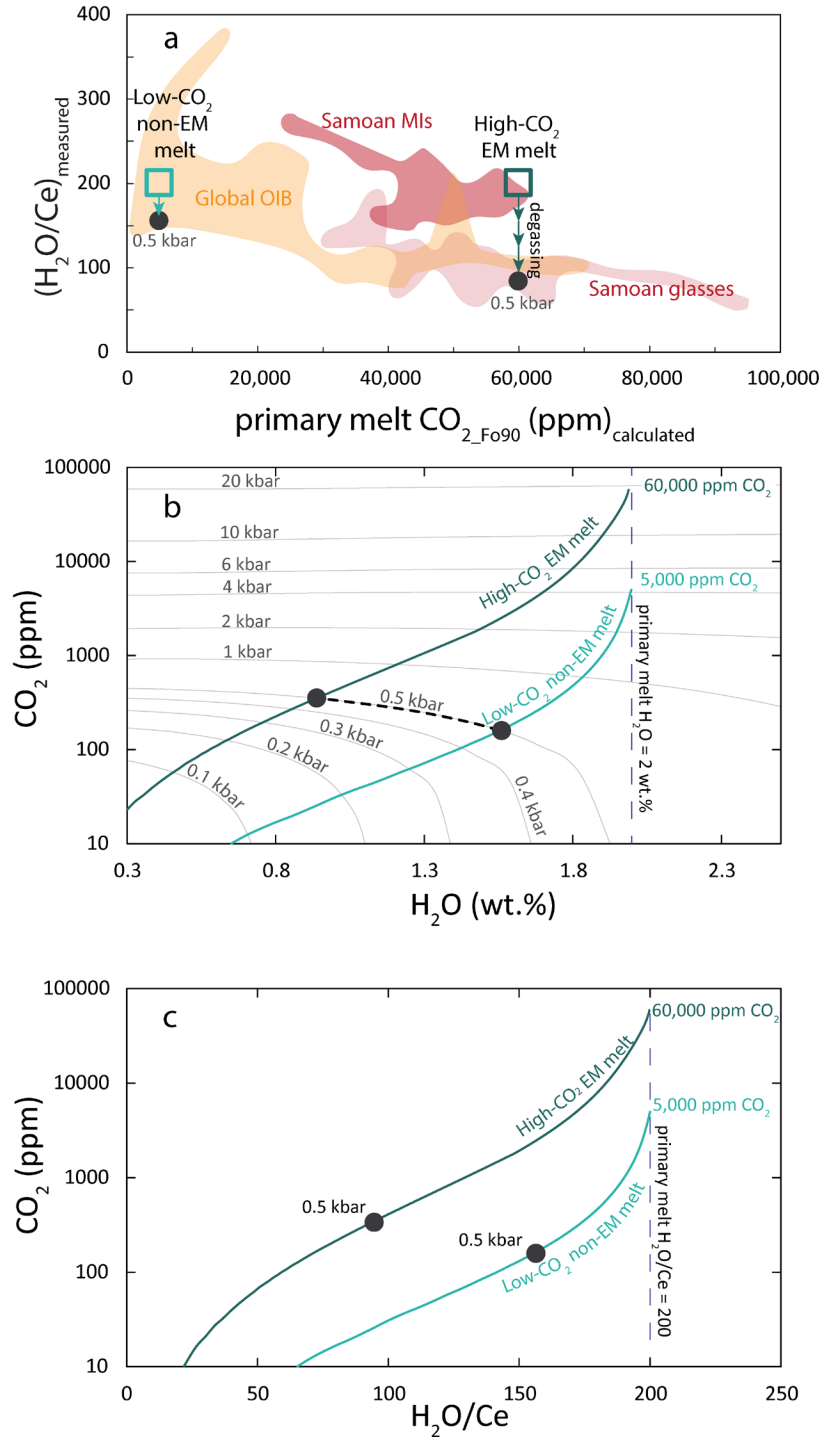
1202



1203

1204 **Figure 9.** (a) Linear fit (blue line) of global MORB and OIB glasses and melt inclusions with respect to  
1205  $\text{CO}_2/\text{Nb}$  and  $(\text{La}/\text{Sm})_N$ . Data compilation is the same as what is presented in Figure 1 of Hirschmann  
1206 (2018). The values for  $\text{CO}_2/\text{Nb}$  and  $(\text{La}/\text{Sm})_N$  in panel (a) are given in Table S10. The blue dashed lines  
1207 represent the 95% prediction interval. The 95% confidence interval of the linear fit is given with the  
1208 equation of the linear fit. The linear relationship calculated in panel a is used to estimate the  $\text{CO}_2/\text{Nb}$   
1209 values for glasses and melt inclusions in Figure 8. (b) Linear fit (blue line) to the Mid-Atlantic Ridge  
1210  $\text{CO}_2/\text{Nb}$  versus  $(\text{La}/\text{Sm})_N$  data from Cartigny et al. (2008). The blue dashed lines are the 95% prediction  
1211 bands for the linear fit using Cartigny et al. (2008) data. Sources of data for panel a: L. Strike (Lucky  
1212 Strike): Wanless et al. (2015); JdF, EPR (Juan de Fuca, East Pacific Rise): Wanless and Shaw (2012);  
1213 Gakkel: Wanless et al. (2014); Siqueiros: Saal et al. (2002); pEMORB and pDMORB (Pacific enriched and  
1214 depleted MORB): Shimizu et al. (2016); UDM (ultra-depleted MORB): Michael and Graham (2015);  
1215 pop.rx (North Atlantic popping rocks): Cartigny et al. (2008); Eq. Atl. (Equatorial Atlantic): Le Voyer et al.  
1216 (2017); Iceland: Hartley et al. (2014), Neave et al. (2014); N. Iceland (Borgarhraun): Hauri et al. (2018); N.  
1217 Arch (North Arch, Hawai'i): Dixon et al. (1997), Frey et al. (2000); Hawai'i (Kīlauea): Anderson and Poland  
1218 (2017); Petit Spot B (Western Pacific seamounts): Machida et al. (2015).

1219



1220

1221 **Figure 10.** Figure illustrating how submarine glasses from enriched mantle (EM) sources acquire low  
 1222 H<sub>2</sub>O/Ce relative to glasses from non-EM sources. We test two melt compositions that are identical in  
 1223 every way (major and trace element compositions are identical and H<sub>2</sub>O is 2 wt.%) except for CO<sub>2</sub>, where  
 1224 one melt starts with 60,000 ppm CO<sub>2</sub> (meant to represent an EM melt) and the other melt starts with  
 1225 5000 ppm CO<sub>2</sub> (meant to represent the non-EM melt). (a) H<sub>2</sub>O/Ce versus primary melt CO<sub>2</sub>, reproduced  
 1226 in cartoon form from Figure 8e. The black circle indicates the H<sub>2</sub>O/Ce value for melts at 0.5 kbar after

1227 degassing. (b) In a plot of CO<sub>2</sub> versus H<sub>2</sub>O, modeled closed system degassing paths show the impact of  
1228 varying initial CO<sub>2</sub> on a melt that has the same initial H<sub>2</sub>O content of 2 wt.%. While both melts start with  
1229 the same initial H<sub>2</sub>O, those with higher initial CO<sub>2</sub> degas more H<sub>2</sub>O and have lower H<sub>2</sub>O at a given isobar  
1230 compared to a melt that has lower initial CO<sub>2</sub>, demonstrating how higher initial CO<sub>2</sub> results in lower H<sub>2</sub>O  
1231 (and lower H<sub>2</sub>O/Ce) in the erupted lavas. Degassing trends assume oxygen fugacity (QFM) and  
1232 temperature (1200°C) and are calculated in rhyolite-MELTS v1.2 using AVON3-78-1#3 major element  
1233 melt inclusion composition. Bottom panel shows the same degassing paths as the upper panels but  
1234 shows H<sub>2</sub>O/Ce instead of H<sub>2</sub>O. Calculation of H<sub>2</sub>O/Ce along the degassing paths assumes 1) an initial  
1235 H<sub>2</sub>O/Ce value of 200 (similar to the average H<sub>2</sub>O/Ce value of Samoan melt inclusions examined here) and  
1236 2) a constant melt Ce concentration (100 ppm) that is calculated using the initial H<sub>2</sub>O/Ce ratio (i.e., 200)  
1237 and the initial H<sub>2</sub>O (2 wt.%). Similar to the relationship between CO<sub>2</sub> and H<sub>2</sub>O for high and low CO<sub>2</sub> melts,  
1238 at a given isobar the melt with high initial CO<sub>2</sub> has significantly lower H<sub>2</sub>O/Ce compared to the melt with  
1239 lower initial CO<sub>2</sub>. Isobars are calculated using MagmaSat for the average Malumalu melt inclusion  
1240 composition at 1200°C. We consider only the case of M=0 to highlight the role of initial CO<sub>2</sub> and  
1241 saturation pressure on the H<sub>2</sub>O content of a glass, and non-zero M values would result in even more  
1242 rapid H<sub>2</sub>O loss.

1243

1244

1245